NASA Technical Memorandum 87591

EFFECTS OF WING MODIFICATION ON AN AIRCRAFT'S AERODYNAMIC PARAMETERS AS DETERMINED FROM FLIGHT DATA

ROBERT ALAN HESS

JANUARY 1986

National Aeronautics and
Space Administration

Langley Research Center
Hampton, Virginia 23665

Summary

A study of the effects of four wing-leading-edge modifications on a general aviation aircraft's stability and control parameters is presented. Flight data from the basic aircraft configuration and configurations with wing modifications are analyzed to determine each wing geometry's stability and control parameters. The parameter estimates and aerodynamic model forms are obtained using the stepwise regression and maximum likelihood techniques. The resulting parameter estimates and aerodynamic models are verified using vortex-lattice theory and by analysis of each model's ability to predict aircraft behavior. Comparisons of the stability and control derivative estimates from the basic wing and the four leading-edge modifications are accomplished so that the effects of each modification on aircraft stability and control derivatives can be determined.

NOMENCLATURE

A	system matrix for state equation
A_0, A_1	model parameters for intermediate step in SF
a_a	lift-curve slope of aileron
a_r	lift-curve slope of rudder
a_F	lift-curve slope of vertical fin
a_X, a_Y, a_Z	longitudinal, lateral, and vertical accelerations, respectively, g units
a_l	lift-curve slope of horizontal stabilator
B	control-distribution matrix for state equation
b	wing span, m
C	state-distribution matrix for the output equation
C_L	lift-force coefficient, $L/\bar{q}S$
C_{L_0}	coefficient of lift at $\alpha = 0°$
C_l	rolling-moment coefficient, $M_X/\bar{q}Sb$
C_m	pitching-moment coefficient, $M_Y/\bar{q}S\bar{c}$
C_n	yawing-moment coefficient, $M_Z/\bar{q}Sb$
C_X	longitudinal-force coefficient, $F_X/\bar{q}S$
C_Y	lateral-force coefficient, $F_Y/\bar{q}S$
C_Z	vertical-force coefficient, $F_Z/\bar{q}S$
$\bar{c}$	mean aerodynamic chord, m
D	control-distribution matrix for the output equation
E{}	expectation operator
e	equation error
F	random variable possessing F-distribution probability density function
F_p	partial F-statistic
F_X, F_Y, F_Z	forces along longitudinal, lateral, and vertical body axes, respectively, N
G	sensitivity matrix
g	acceleration due to gravity, m/sec^2

I_X, I_Y, I_Z	moments of inertia about longitudinal, lateral, and vertical body axes, respectively, kg-m
I_{XZ}	product of inertia, kg-m
i,j	indices of parameters and variables
J	cost function
L	lift force, N
l_{eff}	distance between CG and lateral planform AC, m
l_F	distance between CG and vertical fin AC, m
l_t	distance between CG and horizontal tail AC, m
M_X, M_Y, M_Z	moments about longitudinal, lateral, and vertical body axes, respectively, N-m
m	mass, kg
N	number of samples
n	number of unknown parameters
p	body axis roll-rate, rad/sec or deg/sec
q	body axis pitch-rate, rad/sec or deg/sec
$\bar{q}$	dynamic pressure, $\frac{1}{2}\rho V^2$, N/m^2
R	measurement-noise covariance matrix
R^2	squared multiple correlation coefficient
r	body axis yaw-rate, rad/sec or deg/sec
r_{jy}	partial correlation coefficient for the j^{th} independent variable and dependent variable
S	wing area, m
S_a	aileron area, m
S_T	horizontal tail area, m
s_{yy}, s_{jj}, s_{jy}	sums of squares pertaining to independent and dependent variables
s^2	equation error variance estimate
t	time, sec
U	control-distribution matrix for output equation

u	velocity along longitudinal body axis, m/sec
V	aircraft total velocity, m/sec
V_i, V_j	elements of measurement noise vector
V_H	horizontal tail volume
V_V	vertical tail volume
X	matrix of independent variables or state vector
x_i	i^{th} independent variable
x_L, x_R	left and right longitudinal FDV sensor offset from CG, respectively
x_X, x_Y, x_Z	longitudinal, lateral, and vertical offset of longitudinal accelerometer from CG, respectively, m
Y	dependent variable vector or output variable vector
y	dependent variable
y_a	lateral distance from center of aileron to CG, m
y_L, y_R	left and right lateral FDV sensor offsets from CG respectively, m
y_s	lateral distance from center of semispan to CG, m
y_X, y_Y, y_Z	longitudinal, lateral, and vertical offset of lateral accelerometer from CG, respectively, m
y^*	dependent variable in intermediate step of SR
Z	vector of measured outputs
Z_F	vertical distance from vertical fin AC to CG, m
z_i	i^{th} independent variable in intermediate step of SR
z_L, z_R	left and right vertical FDV sensor offsets from CG, respectively, m
z_X, z_Y, z_Z	longitudinal, lateral, and vertical offset of vertical accelerometer from CG, respectively, m
α	angle of attack, rad or deg
$\alpha_L=0$	angle of attack at zero lift, rad or deg
α_p	confidence level of F-statistic
β	sideslip angle, rad or deg
Γ	wing dihedral, rad or deg

Δ	incremental value
δ_a	aileron deflection, rad or deg
δ_h	horizontal stabilator deflection, rad or deg
δ_{ij}	Kronecker delta
δ_r	rudder deflection, rad or deg
η_1, η_2	degrees of freedom for numerator and denominator of F-statistic, respectively
θ	vector of unknown parameters
θ_i	i^{th} element of vector of unknown parameters
θ	pitch angle, rad or deg
ν	vector of residuals
ρ	air density, kg/m^3
σ	standard error
σ^2	variance of measurement noise or equation error
ϕ	roll angle, rad or deg
ψ	yaw angle, rad or deg

SUBSCRIPTS

CG	center of gravity
E	referenced to fixed earth axis
i,j,k	general indices
L,R	left or right, respectively
low,up	pertaining to lower or upper fuselage, respectively
M	measured
u	referenced to unaccelerated, trimmed flight
0	referenced to zero angle of attack

SUPERSCRIPTS

T	transpose
-1	inverse

$\dot{}$	derivative with respect to time
$'$	parameters include downwash effects
$-$	mean value
$\hat{}$	estimate
$\sim$	non-dimensionalized by factors of $\bar{c}/2V$ or $b/2V$

ABBREVIATIONS

AC	aerodynamic center
CG	aircraft center of gravity
FDV	flow direction and velocity
FLE	full leading-edge
FOLE	faired outboard leading-edge
MARS	miniature attitude reference system
ML	maximum likelihood
NACA	National Advisory Committee for Aeronautics
NASA	National Aeronautics and Space Administration
OLE	outboard leading-edge
SLE	segmented leading-edge
SR	stepwise regression
VL	vortex-lattice

Aerodynamic derivatives referenced to a system of body axes with the origin at the center of gravity (see fig. 1):

$$C_{Z_\alpha} = \frac{\partial C_Z}{\partial \alpha} \qquad C_{Z_q} = \frac{\partial C_Z}{\partial q\bar{c}/2V} \qquad C_{Z_{\delta_h}} = \frac{\partial C_Z}{\partial \delta_h}$$

$$C_{m_\alpha} = \frac{\partial C_m}{\partial \alpha} \qquad C_{m_q} = \frac{\partial C_m}{\partial q\bar{c}/2V} \qquad C_{m_{\delta_h}} = \frac{\partial C_m}{\partial \delta_h}$$

$$C_{Y_\beta} = \frac{\partial C_Y}{\partial \beta} \qquad C_{l_\beta} = \frac{\partial C_l}{\partial \beta} \qquad C_{n_\beta} = \frac{\partial C_n}{\partial \beta}$$

$$C_{Y_p} = \frac{\partial C_y}{\partial pb/2V} \qquad C_{l_p} = \frac{\partial C_l}{\partial pb/2V} \qquad C_{n_p} = \frac{\partial C_n}{\partial pb/2V}$$

$$C_{Y_r} = \frac{\partial C_Y}{\partial rb/2V} \qquad C_{l_r} = \frac{\partial C_l}{\partial rb/2V} \qquad C_{n_r} = \frac{\partial C_n}{\partial rb/2V}$$

$$C_{Y_{\delta_a}} = \frac{\partial C_Y}{\partial \delta_a} \qquad C_{l_{\delta_a}} = \frac{\partial C_l}{\partial \delta_a} \qquad C_{n_{\delta_a}} = \frac{\partial C_n}{\partial \delta_a}$$

$$C_{Y_{\delta_r}} = \frac{\partial C_Y}{\partial \delta_r} \qquad C_{l_{\delta_r}} = \frac{\partial C_l}{\partial \delta_r} \qquad C_{\delta_r} = \frac{\partial C_n}{\partial \delta_r}$$

INTRODUCTION

Unexpected entry of general aviation aircraft into stall and spin flight conditions and the unsatisfactory handling characteristics that result in these regimes are major factors in aircraft accidents and fatalities (ref. 1). As a result of the work done through the NASA General Aviation Stall/Spin program (ref. 2,3), it was indicated that modifications of an aircraft wing's leading-edge promise improved stall/spin characteristics. The previous stall/spin research program included results from spin-tunnel tests, free-flight radio control model tests, full-scale aircraft flight tests, and rotary balance wind tunnel tests. Though various wing modifications were shown to improve the stall/spin characteristics of general aviation aircraft, the majority of this work has been qualitative in nature. In general, these studies either determined modes of instability associated with each type of wing modification, or have determined some of the basic aerodynamic characteristics of each geometry. A complete flight data analysis of the effect of wing-leading-edge modifications on an aircraft's stability and control parameters is of assistance in quantifying which of the various wing-leading-edge modifications would be most favorable for improving the stall/spin charcteristics of such aircraft. Where the previous work was less systematic in nature, this study is an effort to systematically develop complete aerodynamic models for these wing configurations.

In an effort to analyze the effects of wing-leading-edge modifications on an aircraft's stability and control derivatives, a study was completed for a full-scale general aviation aircraft on which wing-leading-edge modifications were placed. Flights were flown in the pre- and post-stall regimes with the angle of attack in the range of between approximately 4 and 24 degrees. The pre-stall regime is defined for this paper as the angle of attack range where 1) the lift curve is nonlinear and 2) α is less than the static stall angle of attack. Post-stall will refer to flight conditions in which α is greater than the static stall angle of attack. The data that resulted from the flight tests was analyzed using the stepwise regression and maximum likelihood techniques. From these analyses, a complete set of stability and control derivatives were estimated. Though there was no wind tunnel data available for comparison, the parameter estimates were verified by using vortex-lattice theory to estimate theoretical stability and control values, and by inspection of the aircraft behavior prediction capabilities of the estimates. The stability and control derivative estimates from each wing geometry were compared and the effects of wing modification on the stall/spin characteristics were determined.

Presented in this paper is a description of the flight test program that was performed, and of the data analysis techniques that were used. Also discussed are the aerodynamic models which were used in the parameter estimation techniques. A discussion of the stability and control derivative estimates is presented along with concluding statements and remarks.

FLIGHT TEST AND DATA COLLECTION

As a continuing project of the NASA General Aviation Stall/Spin program, a variety of general aviation aircraft possessing wing-leading-edge modifications have been flight tested in an effort to improve the stall/spin characteristics of such

aircraft. Data from the flight tests of these aircraft have been collected and made available for analysis by NASA personnel and other researchers working in the area of stall/spin improvement. The data on which this study is based were provided by the staff of the Flight Dynamics Branch of the Low-Speed Aerodynamics Division at the NASA-Langley Research Center.

The flight test program was carried out for a low-wing, single-engine general aviation aircraft. A three view drawing of the test airplane with the basic wing is shown in figure 2. The four different wing-leading-edge modifications were created by adding a drooped section to the basic wing. The resulting modifications are shown in figure 3. They include a wing on which the full leading-edge span was modified by addition of the drooped section (FLE modification), a wing in which a gap was placed in the drooped section, creating a segmented leading-edge (SLE modification), and a wing in which the outboard sections of the span were modified by the droop and a fairing which smoothed the leading-edge from the drooped section to the basic wing (FOLE modification). A wing geometry similar to the FOLE modification but without the faired section was also analyzed. This irregular leading-edge geometry is known as the outboard leading-edge (OLE) wing modification. The physical characteristics of all the aircraft test configurations are presented in table 1.

The test aircraft was fully instrumented to record angular rates, linear accelerations, control deflections, angles of attack and sideslip, true airspeed, engine RPM, attitude angles, and altitude. The linear accelerations were measured by three accelometers mounted orthogonally near the aircraft CG location. Angular rates were measured by three separate rate gyros which were themselves orthogonally mounted. The rudder, aileron, and horizontal stabilator control deflections were measured by position transducers placed near those surfaces. Angles of attack and sideslip and true airspeed were obtained from flow direction and velocity (FDV) sensors, which were mounted on tip booms in front of each wing's leading-edge. The engine RPM was measured via a magnetic pick-up mounted on the engine flywheel. Attitude angles were measured by a three-axis miniature attitude reference system (MARS). The roll and pitch angles are measured with respect to a vertical position of the spin axis. Altitude was sensed by a pressure transducer in the aircraft's static system. Measurements were collected from the instrumentation and digitized at a rate of 20 samples/sec and then stored on magnetic tape.

The flight tests were executed such that the collected data covered a large range of attack and sideslip angles. Longitudinal, quasi-steady, acceleration-deceleration maneuvers were flown along with longitudinal, lateral, and combined large and small amplitude transient maneuvers. The quasi-steady maneuvers were maneuvers in which there was almost no short period excitation ($q \approx 0$) as the pilot very slowly pulls back the stick until a maximum controllable α is achieved, then slowly returns the stick forward until the original trim α is reached. From such maneuvers, one can derive lift and pitching moment curves.

Combined maneuvers involve a mixture of both lateral and longitudinal excitation in the same test maneuver. The longitudinal motion was excited from trimmed conditions by the pilot applying simple stabilator doublets and pulses, while the lateral motion was excited from trimmed conditions by pilot applied sequential aileron-rudder or rudder-aileron inputs. For all the configurations tested, the aircraft was flown with a full aft CG location (31% $\bar{c}$).

The digitized flight data collected from each test configuration was corrected to reflect values referenced to the aircraft CG location and to reflect previously determined instrumentation calibration.

The flow direction and velocity (FDV) sensor measurements were corrected for wing upwash and sidewash. These corrections were determined from flight and wind tunnel tests. The velocity measured from the FDV sensors was corrected to reflect calibration runs flown with the test aircraft. The airplane was flown at various speeds over a measured ground trace. The true velocity as determined by the time required to cover the ground trace was compared to that measured from the FDV sensors and an appropriate linear calibration was determined. This calibration was then applied to obtain corrected airspeed. The angle-of-attack measurements were corrected by analysis of steady-state flight test data. The corrections were extrapolated to higher attack angles through the use of unpublished data obtained in the NASA-Langley 12-foot tunnel.

Many of the measurements from the aircraft instrumentation were not made at or near the aircraft CG location. Therefore, angles of attack and sideslip, velocity, and linear accelerations were subsequently transformed to the aircraft CG location. The left and right boom measurements from the FDV sensors were transformed to the aircraft CG and then averaged together to obtain corrected airspeed and angles of attack and sideslip. The offset of the accelerometer package from the CG was known, hence, the accelerometer measurements were transformed to the CG location. The attitude angle measurements from the MARS gyro package were transformed to Euler angle measurements based on the angles at which the gyros were uncaged. The transformation and calibration equations used in the data correction are given in appendix A.

In an effort to confirm that there were no bias errors in the boom or accelerometer measurements or scale factor errors in the boom measurements, the extended Kalman filter-smoother, fixed-point smoother of reference 4 was applied to the data. If the filter-smoother routine indicated measurement bias/scale factor errors, the data were then corrected so that compatibility between the various measurements existed.

PARAMETER EXTRACTION TECHNIQUES

The successful parametric modeling of the aerodynamics for an airplane operating near stall angles of attack consists of two phases. First, the aerodynamic model structure must be determined and second, the associated aerodynamic parameters (stability and control derivatives) must be estimated. Though the aerodynamic model structure is known to be linear at low angles of attack, the existence of nonlinearities at higher angles of attack has been made known in several recent reports on flight test results, (refs. 8,17,20).

Various methods exist (refs. 5,6,7,22,23) which allow for the determination of aircraft stability and control derivatives from flight data. Two of these methods, stepwise regression (SR) and maximum likelihood (ML), were used in this study. Each method differs in its level of simplicity, optimization criteria, and ability to determine aerodynamic model structure.

Stepwise Regression

Since a large number of possible nonlinear terms could contribute to the aerodynamic function, some method must be developed that examines only the useful terms while ignoring those that are superfluous. One possibility is to look at all combinations of linear and nonlinear terms. However, the number of models to be

considered grows too fast with the number of possible terms for such a technique to be practical. The use of the stepwise regression was suggested in reference 25. The stepwise regression examines each term as to its usefulness in improving the model (by reducing residual variance).

Stepwise regression (ref. 8) belongs to a family of estimation techniques known as equation error methods. Equation error methods, which are based on the least square principle, estimate parameters such that the sum of squares in the difference between the measured aerodynamic forces and moments and those calculated by the estimated parameters is minimized.

In the development of least squares methodology, assume that a dependent variable, y(t), can be closely approximated as a linear combination of independent variables. For an aircraft, the aerodynamic model can be formulated as

$$y(t) = \theta_0 + \theta_1 x_1(t) + \ldots + \theta_{n-1}\, x_{n-1}(t) \tag{1}$$

The dependent variable y(t) represents the aerodynamic force and moment coefficients, θ_1 to θ_{n-1} represent the stability and control derivatives, θ_0 is the value of the aerodynamic force or moment coefficient when the independent variables are zero, and $x_i(t)$ represent the n-1 independent variables, which are composed of the state and control variables or their combinations.

At any particular time, t_i; i = 1,2,...,N, the measured data can be used to approximate equation (1) by

$$y(i) = \theta_0 + \theta_1 x_1(i) + \ldots + \theta_{n-1} x_{n-1}(i) + e(i) \tag{2}$$

Because N observations were made, N linear equations approximating equation (1) result. These approximations contain an equation error term, e(i). Given that the number of observations is greater than the number of unknowns, N > n, the vector of unknown parameters, θ , may be estimated using the method of least squares (ref. 5):

$$\hat{\theta} = (X^T X)^{-1} X^T Y \tag{3}$$

where $\hat{\theta}$ is the n x 1 vector of parameter estimates, X is the N x n concatenated matrix of measured independent variables, and Y is the N x 1 vector of measured dependent variables.

The properties of the least squares estimates depend upon the assumptions postulated about the equation error and the independent variables. Given the assumptions:

1. e is stationary with zero mean

2. e is uncorrelated with X

3. X is deterministic

4. e(i) are independent with mean zero and constant variance σ^2

5. e(i) is normally distributed

then the covariance matrix of parameter estimates will have the form

$$E\{(\theta - \hat{\theta})(\theta - \hat{\theta})^T\} = \sigma^2(X^TX)^{-1} \tag{4}$$

where the variance of the equation error, σ^2, can be estimated by s^2 as given by

$$s^2 = \frac{1}{N-n} \sum_i \hat{e}^2(i) \tag{5}$$

$$\hat{e}(i) = y(i) - \hat{y}(i) \tag{6}$$

given that the dependent variable can be estimated as

$$\hat{y}(i) = \hat{\theta}_0 + \hat{\theta}_1 x_1(i) + \ldots + \hat{\theta}_{n-1} x_{n-1}(i) \tag{7}$$

It should also be noted that in real situations, the previously mentioned assumptions are not, in general, met. Thus, the least squares estimates can be asymptotically biased and can have higher standard errors than those predicted by equation (4).

Before the least square concept is used to formulate the SR method, it will be of importance to define the random variable F which has an F-distribution with degrees of freedom n-1 and N-n as

$$F = \frac{\hat{\theta}^T X^T Y - N\bar{y}^2}{(n-1)\sigma^2} \tag{8}$$

Another important variable is the squared multiple correlation coefficient, R^2, which is found by the relationship

$$R^2 = \frac{\hat{\theta}^T X^T Y - N\bar{y}^2}{Y^T Y - N\bar{y}^2} \tag{9}$$

where the mean value of y is found by

$$\bar{y} = \frac{1}{N} \sum_{i} y(i) \tag{10}$$

The squared multiple correlation coefficient can be related to the variable F by the equation

$$F = \frac{N - n}{n - 1} \frac{R}{1 - R^2} \tag{11}$$

Also of consequence is the test of the significance of individual terms in the regression (partial F-test). A particular parameter, θ_j, is deemed significant if its partial F-test criterion, F_p, given by

$$F_p = \frac{\hat{\theta}_j^2}{s^2(\theta_j)} \tag{12}$$

is greater in value than the tabulated F-distribution, $F(\eta_1, \eta_2, \alpha_p)$, which possesses degrees of freedom $\eta_1 = 1$, $\eta_2 = N-n$, and a significance level α_p (ref. 24).

The stepwise regression procedure is a least squares estimator in which independent variables are inserted into the model, one at a time, until satisfactory results are obtained. The independent variables are inserted into the regression model based upon the partial correlation coefficient of the variables not currently included in the regression equation. Starting with a postulated regression model as in equation (2), the first independent variable for the postulated model is chosen as the one which is most closely correlated with y. The correlation coefficient, r_{jy}, is given by the equation

$$r_{jy} = \frac{s_{jy}}{(s_{jj} s_{yy})^{1/2}} \tag{13}$$

which is composed of the sum of square terms defined as

$$S_{jy} = \sum_{i} [x_j(i) - \bar{x}_j](y(i) - \bar{y}) \tag{14a}$$

$$s_{jj} = \sum_{i} [x_j(i) - \bar{x}_j]^2 \tag{14b}$$

$$s_{yy} = \sum_i [y(i) - \bar{y}]^2 \tag{14c}$$

and where the mean value of x_j is defined as

$$\bar{x}_j = \frac{1}{N} \sum_i x_j(i) \tag{14d}$$

The independent variable, x_j, with the maximum r_{jy} value is first selected for use in the model. If x_j is selected as x_1, then the model is fit to the data by the expression

$$y = \theta_0 + \theta_1 x_1 \tag{15}$$

A new independent variable, z_2, is created by finding the residuals of x_2 after regressing it on x_1. This is done by defining

$$z_2 = A_0 + A_1 x_1 \tag{16}$$

Then z_2 is given by

$$z_2 = x_2 - \hat{A}_0 - \hat{A}_1 x_1 \tag{17}$$

The variables $z_3, z_4, \ldots, z_{n-1}$ are found in a similar way by regressing the variables $x_3, x_4, \ldots, x_{n-1}$ on x_1. A new dependent variable, y^*, is represented by the residuals of y regressed on x_1. Using the model given by equation (16), i.e.,

$$y^* = y - \hat{\theta}_0 - \hat{\theta}_1 x_1 \tag{18}$$

a new set of partial correlations which include the variables y^*, $z_1, \ldots, z_{n-1}$ are formulated. Such partial correlations of z_j and y^* are related to the model containing the variable x_1. The next independent variable added to the regression model is one of the remaining independent variables x_j whose partial correlation is greatest. Again, the same process is completed and the correlations between the residuals of x_j regressed on the inserted independent variables and the residuals of y regressed on the inserted variables are found.

When the partial F-test criterion of equation (12) is applied to the stepwise regression technique, model structure determination can be completed (ref. 8). As regression models are formulated, each variable inserted into the regression model is tested using the partial F-test criterion. If the variable does not meet the

criterion, that variable is dropped from the model. Hence, only statistically significant terms exist in the model, and the structure of the model is revealed. However, it must be noted that the partial F-test criterion can include too many terms in the model (overparameterization). Therefore, other statistical quantities should be taken into account when selecting adequate models. Some of these criteria are:

1. maximizing F
2. maximizing the R^2 coefficient
3. maximizing F_p terms
4. creating a residual sequence which should appear uncorrelated and Gaussian

Because all these criteria cannot simultaneously be met in practice, it then becomes a case of judgement and experience in determining which model is most adequate.

Because the least square estimates are not explicitly functions of time, the independent and dependent variable measurements can be arranged in any order. This concept can be used to partition the measurements. Each partition is created by collecting the measurements into groups based on the values of one or more of the independent variables. Regressional techniques can then be applied to each partitioned set separately. The resulting parameter estimates for each partition then reflect the relationship of the dependent variable to the independent variables for that particular partition. Such a method is useful when large quantities of data are available, and if a statistically useful number of observations are contained in each partition.

Maximum Likelihood

Another method which is well suited for parameter estimation is the maximum likelihood method. In its simplest form, the maximum likelihood (ML) technique is an output error estimation method. Using such methods, parameters are estimated such that the sum of squares in the differences in the measured and calculated outputs is minimized. Whereas the SR method estimates the unknown parameters for each separate equation describing the dependent variable, the ML method must indirectly estimate the unknown parameters by solving a multivariate system.

In the formulation of this method, it is assumed that only the measured outputs are corrupted by noise. The state, output, and measurement equations are, respectively

$$\dot{X} = AX(t) + BU(t) \tag{19}$$

$$Y = CX(t) + DU(t) \tag{20}$$

$$Z_i = Y_i + V_i \qquad , i=1,2,\ldots,N \tag{21}$$

where X, U, Y, and Z are the vectors of the aircraft states, inputs, outputs, and measured outputs respectively, A and B are the system and control-distribution matrices for the state equation, and C and D are the state-distribution and control-distribution matrices for the output equation. It is assumed that the measurement noise has the properties

$$E\{V_i\} = 0 \qquad ; \qquad E\{V_i V_j^T\} = R\delta_{ij}$$

where R is the measurement noise covariance matrix and is initially an unknown.

The maximum likelihood cost function (ref. 6) for the system can be written as

$$J(\theta) = \frac{1}{2} \sum_i (Z_i - \hat{y}_i)^T R^{-1} (Z_i - \hat{Y}_i) + \frac{N}{2} \ln |R^{-1}| \tag{22}$$

where the notation, $\hat{}$, will always refer to the current estimate of the associated variable. R can be estimated by minimizing the cost function with respect to R. This minimization produces

$$\hat{R} = \frac{1}{N} \sum_i V_i V_i^T \tag{23}$$

Equation (23) is substituted into equation (22) and then the cost function can be written as

$$J(\theta) = \sum_i (Z_i - \hat{Y}_i) T \hat{R}^{-1} (Z_i - \hat{Y}_i) + \text{constant} \tag{24}$$

Minimization of equation (24) with respect to the unknown parameters represents a nonlinear estimation problem. There exists several methods for its solution. The most common method used in aeronautical applications is based on the modified Newton-Raphson algorithm (ref. 9). In this algorithm, it is assumed that the output can be approximated as

$$\hat{Y}(\theta) = \hat{Y}(\theta_0) + \frac{\partial \hat{Y}}{\partial \theta}\Big|_{\theta_0} \Delta\theta \tag{25}$$

where θ_0 is some initial estimate of the unknown, and $\Delta\theta$ is the difference between the actual value of the unknown and the initial estimate of the unknown.

The cost function is minimized by differentiation with respect to θ, which yields

$$\frac{\partial J(\theta)}{\partial \theta} = 0 = -\sum_i G_i^T \hat{R}^{-1} \nu + \sum_i G_i \hat{R}^{-1} G_i \Delta\theta \tag{26}$$

where

$$G_i = \frac{\partial Y_K}{\partial \theta_j}\Big|_i \tag{27}$$

are the sensitivity functions and the residuals, ν, are given by

$$\nu_i = Z_i - \hat{Y}_i(\theta_0) \tag{28}$$

Equation (26) is solved for $\Delta\theta$ by writing it in the form

$$\Delta\theta = \left[\sum_i G_i^T \hat{R}^{-1} G_i\right]^{-1} \sum_i G_i^T \hat{R}^{-1} \nu_i \tag{29}$$

The sensitivity function G must be found by integrating the sensitivity equations. Various methods which depend upon direct integration of the sensitivity equations (ref. 9), or on finite difference methods (ref. 10) have been used in the past. The method of reference 11 was employed in this study. In this method, an efficient scheme for estimating sensitivities is employed. This scheme reduces the computational effort required to compute the sensitivities normally associated with the methods used in ref. 9 and 10.

Once $\hat{\Delta\theta}$ is found (as the estimated value of $\Delta\theta$ from eq. (29)), the estimate of the unknown, θ, is found by incrementing θ_0 by $\hat{\Delta\theta}$. Because of the nature of this technique, the estimation process is repeated until the maximum likelihood cost function is minimized.

Because of the difficulty in trying to implement model structure determination capability in the ML technique, it is generally necessary to know the structure of the model in advance. This is in general not a problem because an adequate model structure can be provided by the stepwise regression analysis. Though the ML technique is computationally more difficult, it does provide asymptotically unbiased estimates. The ML technique is not applicable to partitioned data.

AERODYNAMIC MODEL EQUATIONS

Before parameter estimation and model structure determination techniques can be applied, a model describing the aircraft aerodynamics must be formulated. Such a model must not only be complete and realistic, but must also consider the estimation techniques used so that accurate estimates and adequate structure can be determined.

Assuming that the aircraft is free from any unsteady aerodynamic effects, and the body axis system discussed in appendix D is used, the aerodynamic forces and moments of the various aircraft configurations in question can be postulated as

$$C_a = C_a(\alpha) + C_{a_q}(\alpha)\tilde{q} + C_{a_{\delta_h}}(\alpha)\delta_h \qquad ; \quad (a = X, Z, m) \tag{30}$$

and as

$$C_a = C_{a_\beta}(\alpha) + C_{a_p}(\alpha)\tilde{p} + C_{a_r}(\alpha)\tilde{r} + C_{a_{\delta_a}}(\alpha)\delta_a + C_{a_{\delta_r}}(\alpha)\delta_r \; ; \; (a = Y, l, n) \tag{31}$$

In this formulation, the stability and control derivatives are postulated as functions of α only. $C_a(\alpha)$ can include nonlinear functions of α. For example, $C_a(\alpha)$ might comprise the terms C_{a_o}, $C_{a_\alpha}\alpha$, $C_{a_{\alpha^2}}\alpha^2$, or for a simple linear model $C_a(\alpha)$ would only comprise C_{a_o}, $C_{a_\alpha}\alpha$. Furthermore, the time derivatives of α and β are left out of the models due to their near-linear relationships with the remaining variables. It is also assumed that coupling between the longitudinal and lateral aerodynamics is negligible.

The actual aerodynamic models used for estimation depend on the type of data that is analyzed. For the small amplitude maneuvers, the aerodynamic models were postulated as polynomial functions in input and output variables. Large amplitude maneuvers were postulated as polynomial functions of the input and output variables along with spline functions (see ref. 12) in α. The use of data partitioning for data analysis was employed for use in analyzing both small and large amplitude maneuvers.

The basic polynomial aerodynamic models were composed of linear stability and control terms along with terms which represented first and second order variations of each stability and control term with α. Such models were best suited for use in analyzing small amplitude longitudinal and lateral maneuvers. Since each small amplitude maneuver covers only a small range in angle of attack, the functional relationship between the stability and control derivatives and α can be found only by analyzing many maneuvers each of which covers a different range of α.

Because of the aerodynamic nonlinearities commonly associated with large amplitude maneuvers, low order polynomial models may be inadequate to represent the aerodynamics. The nonlinearities in such aerodynamics can be approximated by including higher order terms in the polynomial expressions. However, such expressions often lead to large covariances on the parameter estimates and poor prediction properties for the model. This problem can be avoided by incorporating spline functions in the model. Spline functions (extensively discussed in ref. 12) do not have the problems associated with polynomial modeling because they are non-zero only for prescribed intervals in α. Since each spline function covers a small range of α, the splines defined on these intervals can approximate the nonlinearities over the large α range quite well using low order terms.

Partitioning the measured data with respect to α allows for stability and control parameter estimates to be found from large and small amplitude maneuvers without incurring the problems associated with higher order polynomial models. The data is partitioned with respect to α such that each partition reflects variations of approximately 1° or 2°. For these small variations in α, the stability and control parameters in each partition can be easily approximated as functions of the median value of α in each partition. The stability and control terms from each partition can then be plotted against the median values. Such plots reflect the functional relationships between the stability and control derivative and α.

DISCUSSION OF RESULTS

The flight test program on which this study was based made available statistically useful amounts of data for the determination of each specific wing geometry's stability and control derivatives. To be statistically useful, flight data must contain a large enough number of points and in addition these points must cover all ranges of interest in the independent variables. Such data distribution is required for consistent estimates of trends in and relationships between variables. Because of an engine failure in the test aircraft prior to the end of the planned test period, there were no quasi-steady flight data available for analysis for the basic wing geometry. Also, there were no combined maneuvers available for analysis for both the FOLE and the OLE geometries. Though certain types of maneuvers were not available, in all cases there were large amounts of both longitudinal and lateral data available for both stepwise regression and maximum likelihood analysis. Table 2 lists the numbers of data points (at a sample rate of 20 points per second) available for analysis by maneuver type for each wing geometry.

The nondimensional stability and control derivatives for each wing geometry were found using both the stepwise regression and maximum likelihood techniques. The majority of the available data was analyzed using the stepwise regression technique because the technique was significantly less expensive in terms of computer time than the maximum likelihood method and could be applied to partitioned data. Figure 4 illustrates a comparison between the SR estimates and the ML estimates of the $C'_{m_{\delta_h}}$ derivative for the SLE geometry. Tables 3 and 4 show examples of the typical results given by both estimation schemes. Inspection of the tabulated SR and ML results indicate some differences in the unknown parameter estimates. Whereas the SR estimates could always be found, much difficulty existed in determining the ML estimates wing to high correlations between the estimates. The ML estimates of weak parameters also tended to show large standard errors because of their low sensitivities.

In the analysis of the aircraft, it was assumed that the spinning propeller had negligible effect on the aircraft aerodynamics. However, such an assumption is not valid for an operating propeller which causes thrust effects. Because of such effects, problems can result in estimating the X-force derivatives. Hence, only the vertical and lateral force derivatives and the pitching, rolling and yawing moment derivatives were determined in this work.

The final estimates of the stability and control derivatives for all of the wing geometries studied are shown in figures 5-10. These figures, which represent the functional relationship between the stability and control parameters and α, were obtained by passing a curve through the combined stepwise regression and maximum likelihood estimates. Where the parameters were estimated with little scatter, the

final stability and control parameter curves were created using numerical least squares curve-fitting techniques. For the parameters which had much greater scatter in their estimates, the final curves were obtained by hand-fitting a curve through the parameter estimates.

If possible, stability and control parameters determined from flight data should be compared to estimates obtained from wind-tunnel tests. Since there were no tunnel data suitable for analysis, the final estimates of each wing geometry's stability and control parameters were verified by comparison to the theoretical estimates discussed in appendix B and by analysis of their aircraft behavior prediction capability (discussed in appendix C). Comparison of the theoretical estimates to the flight estimates and comparison between the measured and predicted time histories indicate that the flight data estimates were physically realistic and that the estimated aerodynamic models were adequate.

A discussion of the comparison of the stability and control parameters for the basic, FLE, SLE, and FOLE wing configurations follow, along with a separate comparison between the similar OLE and FOLE geometries.

Vertical Force Parameters

Analysis of the vertical force parameters shown in figure 5 indicates significant differences between the SLE/FOLE and the basic/FLE wing geometries. Both the SLE and FOLE show greater magnitudes in their vertical force coefficients as α increases above 10° as compared to the basic or FLE geometries. Also, the SLE/FOLE configurations tend to indicate less stalling tendency. There also exists greater increases in the magnitude of $C_{Z_{\delta_h}}$ for the SLE/FOLE geometries than for the basic or FLE geometries. Such differences may occur because both the SLE/FOLE wings possess irregular leading-edge geometries which generate vortices into the flow over the upper surface of the span. Such vortices tend to decrease the spread of separation on the upper surface of the wing, thus reducing stalling and separated wake effects.

Pitching Moment Parameters

The pitching moment parameters are presented in figure 6. Inspection of this figure indicates that all the wing geometries possess static stability in pitch at a CG location of 31% $\bar{c}$. Also of interest is the fact that all the configurations analyzed exhibit no ability to fly at trimmed conditions without some negative stabilator deflection. Analysis of the other pitching-moment parameters shows significant differences in the pitch-damping derivative, C'_{m_q}, between each wing geometry. As the aircraft enters the stall regime, all the geometries studied show decreases in C'_{m_q}. However, the FOLE geometry shows a major loss in C'_{m_q} as the stall regime is penetrated. The FOLE along with the basic and SLE geometry's pitch-damping become more negative as the aircraft enters the post-stall flight regime. The stabilator effectiveness exhibited no significant variation between any of the geometries studied. It is usually expected that the trends in $C'_{m_{\delta_h}}$ should follow the trends in $C_{Z_{\delta_h}}$ since the stabilator effectiveness is approximately proportional to the tail lift-curve slope. Since $C'_{m_{\delta_h}}$ is also a function of the downwash slope

at the tail, the tail downwash must be varying to such a degree as to reduce the effect of the tail's lifting force on the stabilator effectiveness. In the future, analysis of the flow-field associated with these modifications, specifically wake-fuselage and wake-tail interaction, can also be of use in explaining the variation in trend between $C_{Z_{\delta_h}}$ and $C'_{m_{\delta_h}}$.

Lateral Force Parameters

Though there were no discernable trend differences in the lateral force parameters between the regular and irregular wing geometries, there were noticeable differences in the magnitudes of the lateral force parameters for each geometry. As figure 7 shows, there were variations in the C_{y_β} derivative between each geometry. The basic wing showed a pronounced loss in magnitude of C_{y_β}, whereas the SLE, FLE, and FOLE configurations indicated less or no decrease in the magnitude of C_{y_β}. For these four geometries, the $C_{y_{\delta_r}}$ derivative generally behaved as expected as the aircraft entered the stall regime, i.e., $C_{y_{\delta_r}}$ decreased in magnitude as angle of attack increased due to wake interaction with the tail. The SLE wing exhibited a drastic drop in $C_{y_{\delta_r}}$ as the aircraft left the stall regime. Upon full penetration into the post-stall regime, the SLE geometry then experienced an increase in $C_{y_{\delta_r}}$. Though the remaining lateral force parameters are generally insignificant and consequently difficult to estimate, both the C_{y_r} and $C_{y_{\delta_a}}$ derivatives for the SLE, FLE, and the FOLE geometries were found. Both the FLE and FOLE configurations had similar $C_{y_{\delta_a}}$ and C_{y_r} derivatives, while the SLE geometry showed major differences in magnitude and sign of these derivatives.

Rolling Moment Parameters

The rolling moment parameters are presented in figure 8. Though there were no significant variations in magnitude in these parameters between wing configuration type (variations less than 20 percent), two derivatives showed variations with respect to leading-edge regularity. The FOLE geometry showed an increase in aileron effectiveness in roll, $C_{l_{\delta_a}}$, of approximately 30 percent along with an increased magnitude in C_{l_p} in the pre-and post-stall flight regimes. Such variations in these modification's rolling characteristics are attributable to reduction in the separated flow over the outboard surface of each irregular geometry's wings.

Yawing Moment Parameters

The yawing moment parameters, illustrated in figure 9, showed major variations with respect to wing geometry. The weathercock stability parameters, C_{n_β}, would in general decrease in magnitude as α increased due to wake-fuselage interaction. This trend is exhibited by the FOLE, FLE and basic wing configurations. The SLE geometry indicated increases in C_{n_β} as the aircraft approached the stall regime. The SLE modification then exhibited a drastic decrease in the weathercock stability as the post-stall regime was penetrated, whereas the FLE, FOLE, and basic geometries exhibited C_{n_β} derivatives of consistent magnitude. Both the irregular leading-edge geometries possessed greater rudder effectiveness parameters, $C_{n_{\delta_r}}$, than the FLE or basic wing configurations. Of special interest was the basic wing which possessed total loss of rudder effectiveness as α approached 23°. The yaw-damping parameter, C_{n_r}, was only identifiable in the pre-stall flight regime for the basic wing geometry. All the geometries studied showed loss in yaw damping as α increased, with total loss in yaw damping occurring for the SLE geometry at $\alpha = 17°$, and total loss in C_{n_r} for the FLE geometry occurring at $\alpha = 23°$. The yaw due to roll parameter, C_{n_p}, was also not well identifiable for the basic wing configuration. Though the FLE and FOLE geometries showed similar trends in C_{n_p}, the SLE configuration exhibited large variations in magnitude in C_{n_p} as α increased.

Comparison of OLE and FOLE Geometries

Figure 10 illustrates the variation in the stability and control parameters with α for the OLE and FOLE modified wing geometries. Because both geometries are very similar, major differences in the values of the stability and control derivatives for these geometries would not be expected, and analysis of these estimates confirms this. Though there were variations of approximately 15 percent between the parameters of the OLE and FOLE geometries, only the $C_{Z_{\delta_h}}$ derivative showed any major differences in magnitude (but not in trend). The $C_{Z_{\delta_h}}$ parameter for the OLE geometry was 30 percent smaller than that of the FOLE configuration for the pre-stall regime, and there existed up to a 50 percent decrease in $C_{Z_{\delta_h}}$ for the OLE geometry in the post-stall regime as compared to the FOLE wing. This variation in $C_{Z_{\delta_h}}$ is again attributed to the variation in the wing wake caused by each irregular leading-edge modification's induced vortices.

CONCLUSIONS

The effects of wing-leading-edge modification on a general aviation aircraft's stability and control parameters have been presented. The modifications consist of varying the geometry of the leading-edge by addition of various drooped sections. Flight data were analyzed using two parameter extraction techniques for five different wing geometries (the basic wing and four configurations possessing leading-edge modifications). The analysis of the flight data resulted in complete,

verifiable sets of estimates for each wing geometry's stability and control parameters for $4° < \alpha < 24°$. From comparison of these stability and control parameters, the following points were noted:

(1) The basic wing suffers from loss of lift due to stalling and the resulting loss of roll-damping and weathercock stability. This could result in less than favorable stall/spin characteristics.

(2) The full leading-edge (FLE) modification experiences the same problems in lift and stability as the basic wing. The results indicate that the FLE wing provides no mechanism for the improvement of stall/spin characteristics.

(3) The segmented leading-edge (SLE) wing configuration exhibits reduced weathercock stability and roll-damping for angles of attack greater than 20°. However, the SLE wing can have better stall/spin characteristics than the basic or FLE wings because of its improved flow over the wing surface.

(4) The faired outboard leading-edge (FOLE) modification suffers from poor pitch-damping as the aircraft enters the stall regime. However, this modification can provide the best stall/spin characteristics of all the modifications tested because of its improved lift, roll-damping, and weathercock stability parameters.

(5) The outboard leading-edge (OLE) and FOLE wing configurations possess very similar stability and control parameters owing to similarity in their geometries.

In the final analysis, complete models of aircraft aerodynamics for each of the geometries studied were determined. A systematic study of these configurations has shown quantitatively that the geometries which possess irregular leading-edge geometries are most favorable for improving the stall/spin characteristics of general aviation aircraft.

APPENDIX A

DATA CORRECTION EQUATIONS

I. Upwash/sidewash correction equations for FDV sensors in degrees and knots are

$$\alpha_{B,L} = -1.597 + 0.8196\alpha_{L,M} \tag{A1}$$

$$\alpha_{B,R} = -0.9003 + 0.8196\alpha_{R,M} \tag{A2}$$

$$\beta_{B,L} = \beta_{L,M} \tag{A3}$$

$$\beta_{B,R} = \beta_{R,M} \tag{A4}$$

$$V_{B,L} = -2.757 + 1.0449V_{L,M} \tag{A5}$$

$$V_{B,R} = -1.946 + 1.0160V_{R,M} \tag{A6}$$

II. Transformation of left and right boom velocity measurements to aircraft CG location

$$u_L = V_{B,L}\cos\beta_{B,L}\cos\alpha_{B,L} - qz_L + ry_L \tag{A7}$$

$$u_R = V_{B,R}\cos\beta_{B,R}\cos\alpha_{B,R} - qz_R + ry_R \tag{A8}$$

$$v_L = V_{B,L}\sin\beta_{B,L} - rx_L + pz_L \tag{A9}$$

$$v_R = V_{B,R}\sin\beta_{B,R} - rx_R + pz_R \tag{A10}$$

$$w_L = V_{B,L}\cos\beta_{B,L}\sin\alpha_{B,L} - py_L + qx_L \tag{A11}$$

$$w_R = V_{B,R}\cos\beta_{B,R}\sin\alpha_{B,R} - py_R + qx_R \tag{A12}$$

$$V_L = (u_L^2 + v_L^2 + w_L^2)^{1/2} \tag{A13}$$

$$V_R = (u_R^2 + v_R^2 + w_R^2)^{1/2} \tag{A14}$$

III. Transformation to obtain resultant velocity, attack and sideslip angles, and linear accelerations at aircraft CG location

$$V = 1/2(V_L + V_R) \tag{A15}$$

$$\alpha = 1/2 \left[\tan^{1-} \frac{w_L}{u_L} + \tan^{-1} \frac{w_R}{u_R}\right] \tag{A16}$$

$$\beta = 1/2 \left[\sin^{-1} \frac{v_L}{V_L} + \sin^{-1} \frac{v_R}{V_R}\right] \tag{A17}$$

$$a_X = a_{X_M} + [(q^2 + r^2)x_X - (pr - \dot{r})y_X - (pr - \dot{q})z_X] \tag{A18}$$

$$a_Y = a_{Y_M} + [(p^2 + r^2)y_Y - (pq + \dot{r})x_Y + (qr - \dot{p})z_Y] \tag{A19}$$

$$a_Z = a_{Z_M} + [(q^2 + p^2)z_Z - (pr + \dot{q})x_Z - (qr + \dot{p})y_Z] \tag{A20}$$

IV. Calculation of the orientation of the gyro inertial reference system based on accelerometer measurements for straight and level unaccelerated flight.

$$\psi_u \equiv 0 \tag{A21}$$

$$\theta_u = \sin^{-1}(a_{X_u}) \tag{A22}$$

$$\phi_u = \sin^{-1}(-a_{Y_u}/\cos\theta_u) \tag{A23}$$

V. Transformation of measured attitude angles to Euler angles based on the gyro inertial reference system and the measured attitude angles

$$\theta = \sin^{-1}((\sin\theta_u\cos\theta_M\cos\psi_M - \sin\phi_u\cos\theta_U\cos\theta_M\sin\psi_M) + \cos\phi_u\cos\theta_u\sin\theta_M) \tag{A24}$$

$$\sin\phi_M\cos\theta = \sin\theta_u(\sin\psi_M\cos\phi_M - \sin\phi_M\sin\theta_M\cos\psi_M) + \sin\phi_u\cos\theta_u(\sin\psi_M\sin\theta_M\sin\phi_M + \cos\psi_M\cos\phi_M) + \cos\phi_u\cos\theta_u\sin\phi_u\cos\theta_M \tag{A25}$$

$$\cos\phi_M\cos\theta = -\sin\theta_u(\cos\psi_M\cos\phi_M\sin\theta_M + \sin\psi_M\sin\phi_M) + \sin\phi_u\cos\theta_u(\sin\psi_M\cos\phi_M\sin\theta_M - \cos\psi_M\sin\phi_M) + \cos\phi_u\cos\theta_u\cos\phi_M\cos\theta_M \tag{A26}$$

$$\phi = \tan^{-1}\frac{\sin\phi_M\cos\theta}{\sin\phi_M\cos\theta} \tag{A27}$$

$$\sin\psi_M\cos\theta = \cos\phi_u\cos\theta_M\sin\psi_M + \sin\phi_u\sin\theta_M \tag{A28}$$

$$\cos\psi_M\cos\theta = \cos\theta_u\cos\theta_M\cos\psi_M + \sin\phi_u\sin\theta_u\cos\theta_M\sin\psi_M - \cos\phi_u\sin\theta_u\sin\theta_M \tag{A29}$$

$$\psi = \tan^{-1}\frac{\sin\psi_M\cos\theta}{\cos\psi_M\cos\theta} \tag{A30}$$

APPENDIX B

THEORETICAL PARAMETER ESTIMATES

Theoretical estimates of aircraft stability and control parameters were obtained from consideration of aircraft geometry. The knowledge of each aircraft's planform, wing camber, and control surface locations allowed for the determination of basic aerodynamic characteristics by use of vortex-lattice (VL) methodology. The vortex-lattice analysis was completed using a FORTRAN program (14) which determined aerodynamic forces and moments by modeling the aircraft as a 3-D planform on which horseshoe vortices were placed. An example of the planform representation of the aircraft is presented in figures 11(a-b). The longitudinal stability and control parameters along with one lateral stability parameter were obtained from the planform in figure 11(a), while the remaining lateral stability and control parameters were obtained from the planform represented in figure 11(b).

Because of the nature of the vortex-lattice program, the complex planforms represented by each different wing-leading-edge geometry can be easily modeled. This was a benefit since standard empirical methods (ref. 15) cannot account for the irregular geometries that wing-leading-edge modifications possess. However, because vortex-lattice methods are based on potential flow theory, viscous effects are unaccounted for. Hence, lift coefficients are of larger magnitude than in actual flight conditions and separated wake interactions with the fuselage and tail do not exist. Since the theoretical estimates are only valid for attached flow (α up to 8°), and also since the propeller's ability to augment the lift is not considered, the theoretical study is generally most useful in estimating the order of magnitudes of the various parameters.

The basic aerodynamic characteristics computed from the vortex-lattice analysis were coupled with the aircraft stability and control theory presented in references 16-21 to arrive at a set of linear stability and control parameters.

Owing to difficulty in modeling the proper horseshoe vortex arrangement for the SLE wing geometry, theoretical estimates of that geometry's longitudinal parameters were not obtained. Furthermore, only the lateral parameters of the basic wing configuration were found since the lateral planform cannot model the various wing-leading-edge geometries.

The following formulae were used to obtain the stability and control parameter estimates:

LONGITUDINAL

The vortex-lattice program computes C_{L_α}, C_{m_q}, $\alpha_{L=0}$, C_{L_q}, and C_{l_p}. Hence, for small α, then

$$C_{Z_\alpha} \approx -C_{L_\alpha} \tag{B1}$$

$$C_{Z_q} \approx -C_{L_q} \tag{B2}$$

$$C_{m_\alpha} \approx \frac{\partial C_m}{\partial C_L} C_{L_\alpha} \tag{B3}$$

Since the tail is a horizontal stabilator, the change in lift in the aircraft with respect to tail deflection equals the scaled tail lift-curve slope. Using the VL program to the model the tail, the tail lift-curve slope, a_1 is computed. Hence

$$C_{Z_{\delta_h}} = - \frac{S_T}{S} a_1 \tag{B4}$$

$$C_{m_{\delta_h}} = - V_H a_1 \tag{B5}$$

To account for wing-wake downwash, the downwash slope, $\partial\epsilon/\partial\alpha$, was computed from a theoretical method presented in reference 18. Accounting for wing-wake then results in the equations

$$C_{m_\alpha^\bullet} = - 2V_H a_1 \frac{l_t}{\bar{c}} \frac{\partial \epsilon}{\partial \alpha} \tag{B6}$$

$$C'_{m_\alpha} = C_{m_\alpha} + \frac{\rho S \bar{c}}{4m} C_{m_\alpha^\bullet} C_{L_\alpha} \tag{B7}$$

$$C'_{m_q} = C_{m_q} + C_{m_\alpha^\bullet} \left(1 + \frac{\rho S \bar{c}}{4m} C_{Z_q}\right) \tag{B8}$$

$$C'_{m_{\delta_h}} = C_{m_{\delta_h}} + \frac{\rho S \bar{c}}{4m} C_{m_\alpha^\bullet} C_{Z_{\delta_h}} \tag{B9}$$

LATERAL

The lateral stability and control parameters, being based on the nonsymmetric lateral planform, are generally more difficult to estimate than the longitudinal stablity and control parameters. Because the VL program used in this study must deal with symmetric planform geometries, the upper and lower surfaces and vertical tail are each modeled separately (see fig. 11(b)). Such a method is discussed in reference 19. The analysis of upper and lower fuselage surfaces yields

$$C_{Y_\beta} = C_{Y_{\beta_{up}}} + C_{Y_{\beta_{low}}} \tag{B10}$$

$$C_{Y_p} \simeq 2 \frac{z_F}{b} a_F \tag{B11}$$

$$C_{Y_r} \simeq -2 \frac{l_t}{b} a_F \tag{B12}$$

$$C_{Y_{\delta_a}} = - \frac{S_a}{S} a_a \sin\Gamma \tag{B13}$$

$$C_{Y_{\delta_r}} = a_r \frac{S_r}{S} \tag{B14}$$

The weathercock stability parameter, C_{n_β}, is generally a function of C_{Y_β} and the distance between the lateral center of pressure and the aircraft's CG location. The aircraft's lateral center of pressure can be approximated as the center of area of the lateral planform. Completing the theoretical analysis then results in

$$C_{n_\beta} = - \frac{l_{eff}}{b} C_{Y_\beta} \tag{B15}$$

$$C_{n_p} = - \frac{l_F}{b} C_{Y_p} \tag{B16}$$

$$C_{n_r} = \frac{l_F}{b} C_{Y_r} \tag{B17}$$

$$C_{n_{\delta_a}} = - \frac{y_a}{b} C_{Y_{\delta_a}} \tag{B18}$$

$$C_{n_{\delta_r}} = -a_r \frac{S_r}{S} \frac{l_F}{b} \tag{B19}$$

$$C_{l_\beta} = -\frac{z_F}{b} C_{Y_\beta} \tag{B20}$$

$$C_{l_r} = \frac{z_F}{b} C_{Y_r} \tag{B21}$$

$$C_{l_{\delta_r}} = \frac{z_F}{b} C_{Y_{\delta_r}} \tag{B22}$$

$$C_{l_{\delta_a}} = \frac{y_s}{2b\delta_a} \left[C_{L_0}\big|_{\delta_a} - C_{L_0}\big|_{-\delta_a}\right]\big|_{\delta_a = \delta_{a_1}} \tag{B23}$$

where δ_{a_1} is any aileron deflection at which C_{L_0} can be determined.

The theoretical estimates of each modification's stability and control derivatives are presented in tables 5 and 6. Plots illustrating the comparison between the flight and VL estimates of representative stability and control derivatives are presented in figures 12(a-b). Inspection of these figures and comparison between the tabulated VL estimates (tables 5-6) and the flight estimates (figs. 5-10) indicate very good agreement in magnitude between both sets of estimates. This indicates that the flight data estimates are physically realistic.

APPENDIX C

MODEL/PARAMETER VERIFICATION VIA PREDICTION CAPABILITY ANALYSIS

The estimated aerodynamic models were verified by analyzing how well the models could predict aircraft response to known control inputs. Knowing an adequate model, the prediction should match the actual aircraft response to the control inputs. This also is useful as a check on the estimated stability and control derivatives, since they are incorporated into the aerodynamic models.

A 6-DOF aircraft response is generally predicted by integrating equations D1-D8 using some numerical method. This requires that the initial condition of the states, the complete time history of the control inputs, and the equations for aerodynamic force and moment coefficients as functions of the aircraft states and controls are known. This information is directly available from the stability and control parameters and from the digitized flight data.

In order to simplify the analysis of the aircraft, it was assumed that the spinning propeller had negligible effect on the aircraft's aerodynamics. However, in actual flight conditions, the propeller is not free but spins at the idle engine power RPM. This causes thrust which affects the longitudinal force on the aircraft, which in turn affects the longitudinal velocity, u. Since the thrust effect of the propeller was not known, the longitudinal velocity was taken as a known state from the flight data. Therefore, only a 5-DOF system remained which was solved by integrating equations D2-D8. The integration was completed using a fourth order Runge-Kutta scheme.

Examples of the predicted and measured aircraft response from this analysis are shown in figures 13(a-b). The measured data used in comparison to the response predicted from the estimated models was itself not incorporated in the parameter estimation. As inspection of these figures indicates, the prediction capabilities of the estimated models are quite satisfactory, thereby verifying the adequacy of the estimated aerodynamic models.

APPENDIX D

EQUATIONS OF MOTION

Figures 1 and 14 illustrate the body-axis system along with the directions of the velocities and angular rates and the Euler angles neccessary to describe the motion of an aircraft. Under the following assumptions

1. The airplane is a rigid body
2. The effect of the spinning propeller is negligible
3. The airplane has a plane of symmetry in the XZ plane
4. The rotation of the earth is neglected

the equations which explain the motion of an aircraft are:

$$\dot{u} = -qw + rv - g \sin\theta + \frac{\rho V^2 S}{2m} C_X \tag{D1}$$

$$\dot{v} = -ru + pw + g \cos\theta \sin\phi + \frac{\rho V^2 S}{2m} C_Y \tag{D2}$$

$$\dot{w} = -pv + qu + g \cos\theta \cos\phi + \frac{\rho V^2 S}{2m} C_Z \tag{D3}$$

$$\dot{p} = qr \frac{I_Y - I_Z}{I_X} + \frac{I_{XZ}}{I_X}(pq - \dot{r}) + \frac{\rho V^2 Sb}{2I_X} C_l \tag{D4}$$

$$\dot{q} = pr \frac{I_Z - I_X}{I_Y} + \frac{I_{XZ}}{I_X}(r^2 - p^2) + \frac{\rho V^2 S\bar{c}}{2I_Y} C_m \tag{D5}$$

$$\dot{r} = pq \frac{I_X - I_Y}{I_Z} + \frac{I_{XZ}}{I_X}(\dot{p} - qr) + \frac{\rho V^2 Sb}{2I_Z} C_n \tag{D6}$$

$$\dot{\theta} = q \cos\phi - r \sin\phi \tag{D7}$$

$$\dot{\phi} = p + (q \sin\phi + r \cos\phi) \tan\theta \tag{D8}$$

REFERENCES

1. Silver, Brent W.: Statistical Analysis of General Aviation Stall Spin Accidents. Soc. Automot. Eng. Report No. 760480, Apr. 1976.

2. Staff of Langley Research Center: Exploratory Study of the Effects of Wing-Leading-Edge Modifications on the Stall/Spin Behavior of a Light General Aviation Airplane. NASA TP-1589, Dec. 1979.

3. Newsom, W. A. Jr., Satran, D. R., Johnson, J. L. Jr.: Effects of Wing-Leading-Edge Modifications on a Full-Scale, Low-Wing General Aviation Airplane. NASA TP-2011, June 1982.

4. Klein, V., Scheiss, J. R.: Compatibility Check of Measured Aircraft Response Using Kinematic Equations and Extended Kalman Filter. NASA TN D-8514, Aug. 1977.

5. Klein, V.: "Identification Evaluation Methods," Parameter Identification, AGARD-LS-104, 1979.

6. Klein, V.: System Parameter Identification in Aircraft Dynamics. von Karman Institute for Fluid Dynamics, Lecture Series 80, Aircraft Stability and Control, May 12-16, 1975, Vol. II.

7. Maine, Richard E., Illif, Kenneth W.: Identification of Dynamic Systems. NASA RP-1138, Feb. 1985.

8. Klein, V., Batterson, J. G., Murphy, P. C.: Determination of Airplane Model Structure from Flight Data by Using Modified Stepwise Regression. NASA TP-1916, Oct. 1981.

9. Grove, R. D., Bowles, R. L., Mayhew, S. C.: A Procedure for Estimating Stability and Control Parameters from Flight Test Data Using a Maximum Likelihood Method Employing Real-Time Digital System. NASA D-6735, 1972.

10. Trankle, T. L., Vincent, J. H., Franklin, S. N.: Recent Methods for Non-Linear System Identification. AIAA-81-1865, Aug. 1981.

11. Murphy, P. C.: An Algorithm for Maximum Likelihood Estimation Using an Efficient Method for Approximating Sensitivities. NASA TP-2311, June 1984.

12. Klein, V., Batterson, J. G.: Determination of Airplane Model Structure from Flight Data Using Splines and Stepwise Regression. NASA TP-2126, March 1983.

13. Mulcay, W. J., Rose, R. A.: Rotary Balance Data for a Typical Single-Engine General Aviation Design for an Angle of Attack Range of 8° to 90°. NASA CR-3200, Oct. 1980.

14. Margason, R. J., Lamar, J. E.: Vortex-Lattice Fortran Program for Estimating Subsonic Aerodynamic Characteristics of Complex Planforms. NASA TN D-6142, Feb. 1971.

15. "Light and General Aviation Aerodynamics," Engineering Sciences Data Unit, Vol. 1-4, 1981.

16. Campbell, J. P., McKinney, M. O.: Summary of Methods for Calculating Dynamic Lateral Stability and Response and for Estimating Lateral Stability Derivatives. NACA Report 1098, 1952.

17. Etkin, Bernard: Dynamics of Atmospheric Flight. John Wiley and Sons, 1972.

18. Silverstein, A., Katzoff, S.: Design Charts for Predicting Downwash Angles and Wake Characteristics Behind Plain and Flapped Wings. NACA Report 648, 1939.

19. Sim, A. G., Curry, R. E.: Flight-Determined Stability and Control Derivatives for the F-111 TACT Research Aircraft. NASA TP-1350, Oct. 1978.

20. Klein, V.: Determination of Stability and Control Parameters of a Light Airplane From Flight Data Using Two Estimation Methods. NASA TP-1306, Mar. 1979.

21. Silverstein, A., Katzoff, S., Bullivant, W. K.: Downwash and Wake Behind Plain and Flapped Airfoils. NACA Report 651, 1939.

22. Methods for Aircraft State and Parameter Estimation, AGARD Conference Proceedings No. 172 - AGARD-CP-172, 1975.

23. Parameter Identification, AGARD Lecture Series No. 104 - AGARD-LS-104, 1979.

24. Draper, N. R., and Smith, H.: Applied Regression Analysis. John Wiley and Sons, Inc., 1966.

25. Gupta, Narendra K. and Hall, W. Earl, Jr.: Model Structure Determination and Test Input Selection for Identification of Nonlinear Regimes. ONR-CR215-213-5, U.S. Navy, Feb. 1976. (Available from DTIC as AD A037 831).

TABLE 1.- AIRCRAFT GEOMETRY, MASS AND INERTIA CHARACTERISTICS

	Basic	FLE	SLE	FOLE	OLE
Wing (Modified NACA 63_2A415)					
Area, m^2	13.56	13.61	13.74	13.59	13.59
Aspect ratio	7.395	7.318	7.249	7.329	7.329
Span, m	9.98	9.98	9.98	9.98	9.98
Mean aerodynamic chord, m	1.34	1.39	1.38	1.40	1.37
Dihedral, deg			+ 6.5		
Root incidence, deg			+ 3.		
Tip incidence, deg			+ 1.		
Aileron area (each), m^2			.94		
Aileron span (each), m			1.65		
Aileron deflections, deg			-20/+10		
Stabilator (NACA $63A_1012$)					
Area, m^2			2.516		
Aspect ratio			4.33		
Span, m			3.302		
Mean aerodynamic chord, m			.762		
Tail length, m			4.383		
Tail volume			.607		
Deflections, deg			-15/+2		
Vertical tail (NACA $63A_1012$)					
Area, m^2			1.356		
Aspect ratio			1.46		
Span, m			1.405		
Mean aerodynamic chord, m			1.023		
Tail length, m			4.138		
Tail volume			.041		
Rudder area, m^2			.429		
Rudder root chord, m			.374		
Rudder tip chord, m			.318		
Rudder deflections, deg			+/-25		
Mass					
Flight averaged, kg	1100	1060	1069	1015	1082
Inertia (flight averaged)					
I_X, $kg-m^2$	2245	2351	2406	2319	2380
I_Y, $kg-m^2$	3168	3067	2618	2457	3016
I_Z, $kg-m^2$	4109	4846	4455	4193	4876
I_{XZ}, $kg-m^2$	157	172	168	180	176

TABLE 2.- TABULATED NUMBERS OF DATA POINTS AVAILABLE FOR ANALYSIS

	Wing configuration				
Maneuver type	Basic	FLE	SLE	FOLE	OLE
Longitudinal	5800	7700	4400	6800	7700
Lateral	4600	27000	3000	12000	13000
Combined	2600	3300	6300	*	*
Quasi-steady	*	4500	3600	4800	2100

*No data available.

TABLE 3.- PARAMETER ESTIMATES AND THEIR STANDARD ERROR AS DETERMINED BY SR AND ML FOR A LONGITUDINAL MANEUVER

FLE Wing Geometry
(flight 185, record 13a, $0° < \alpha < 9°$)

	SR Estimates		ML Estimates	
Parameter	Value	Standard error	Value	Cramer-Rao lower bound standard error
C_{Z_0}	-.22	---	-.62	.002
C_{Z_α}	-3.99	.019	-4.23	.079
C_{Z_q}	-12.6	.41	-3.	1.23
$C_{Z_{\delta_h}}$	-.62	.022	-.71	.064
C'_{m_0}	-.072	---	*	*
C'_{m_α}	-.025	.0091	-.049	.0042
C'_{m_q}	-15.1	.20	-16.1	.48
$C'_{m_{\delta_h}}$	-1.86	.011	-1.93	.023

*After second pass through program, C'_{m_0} was $< 10^{-3}$, therefore C'_{m_0} was set to zero to decrease computational effort.

TABLE 4.- PARAMETER ESTIMATES AND THEIR STANDARD ERROR AS DETERMINED BY SR AND ML FOR A LATERAL MANEUVER

SLE Wing Geometry
(flight 124, record 24a, $0° < \alpha\ 12°$)

	SR Estimates		ML Estimates	
Parameter	Value	Standard error	Value	Cramer-Rao lower bound standard error
C_{Y_β}	-.34	.005	-.35	.008
C_{Y_r}	-.80	.044	*	*
$C_{Y_{\delta_a}}$	.17	.012	-.04	.017
$C_{Y_{\delta_r}}$	-.062	.0077	-.04	.016
C_{l_β}	-.084	.0015	-.085	.0056
C_{l_p}	-.390	.0067	-.494	.0033
C_{l_r}	.32	.013	.14	.004
$C_{l_{\delta_a}}$	-.182	.0035	-.19**	---
$C_{l_{\delta_r}}$	.024	.0022	.016	.0008

*Poor or non-existent estimates due to low sensitivities.
**Due to high correlation with other parameters, a fixed estimate was supplied based on SR estimates.

TABLE 4.- Concluded

Parameter	SR Estimates		ML Estimates	
	Value	Standard error	Value	Cramer-Rao lower bound standard error
C_{n_β}	.020	.0016	.035	.0003
C_{n_p}	-.157	.0070	-.056	.0024
C_{n_r}	-.14	.013	-.139	.0013
$C_{n_{\delta_a}}$	*	*	.0023	.00075
$C_{n_{\delta_r}}$	-.047	.0023	-.046	.0004

*No estimate obtained due to insignificance of this parameter.

TABLE 5.- THEORETICAL ESTIMATES OF LONGITUDINAL PARAMETERS (31% $\bar{c}$)

Parameter	Basic	FLE	OLE
C_{Z_0}	-.444	-.434	-.508
C_{Z_α}	-5.394	-5.474	-5.403
C_{Z_q}	-11.427	-11.472	-11.282
$C_{Z_{\delta_h}}$	-.697	-.697	-.697
C'_{m_α}	-.304	-.118	-.259
C'_{m_q}	-22.237	-22.170	-22.132
$C'_{m_{\delta_h}}$	-2.288	-2.288	-2.288

TABLE 6.- THEORETICAL LATERAL PARAMETER ESTIMATES FOR BASIC WING CONFIGURATIONS

Parameter	Value	Parameter	Value	Parameter	Value
C_{Y_β}	-.477	C_{l_β}	-.096	C_{n_β}	.070
C_{Y_p}	*	C_{l_p}	-.540	C_{n_p}	-.065
C_{Y_r}	.396	C_{l_r}	.079	C_{n_r}	-.164
$C_{Y_{\delta_a}}$	-.034	$C_{l_{\delta_a}}$	-.183	$C_{n_{\delta_a}}$	.037
$C_{Y_{\delta_r}}$	.143	$C_{l_{\delta_r}}$	.029	$C_{n_{\delta_r}}$	-.059

*Generally insignificant.

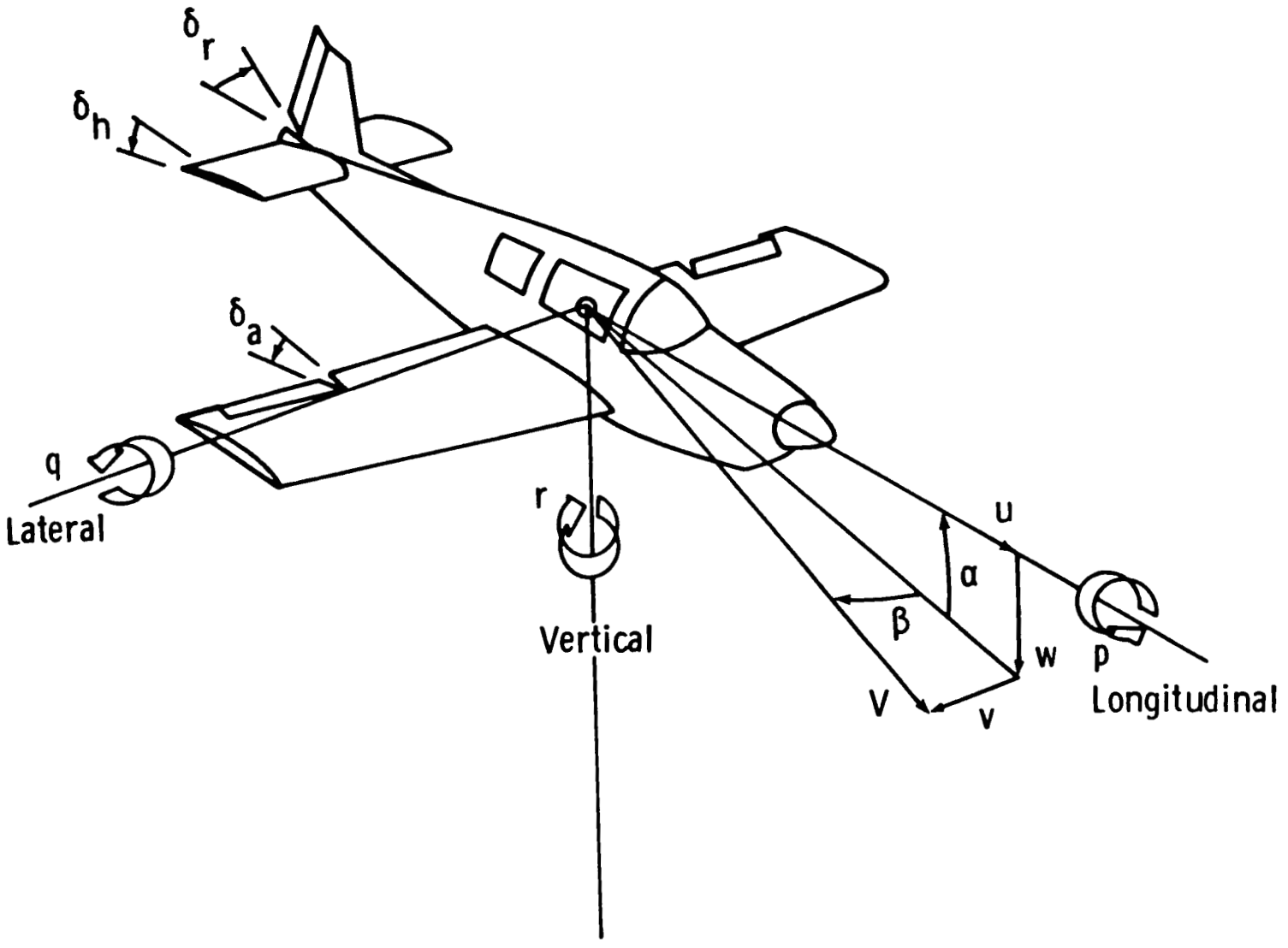

Figure 1.- Body System of Axes

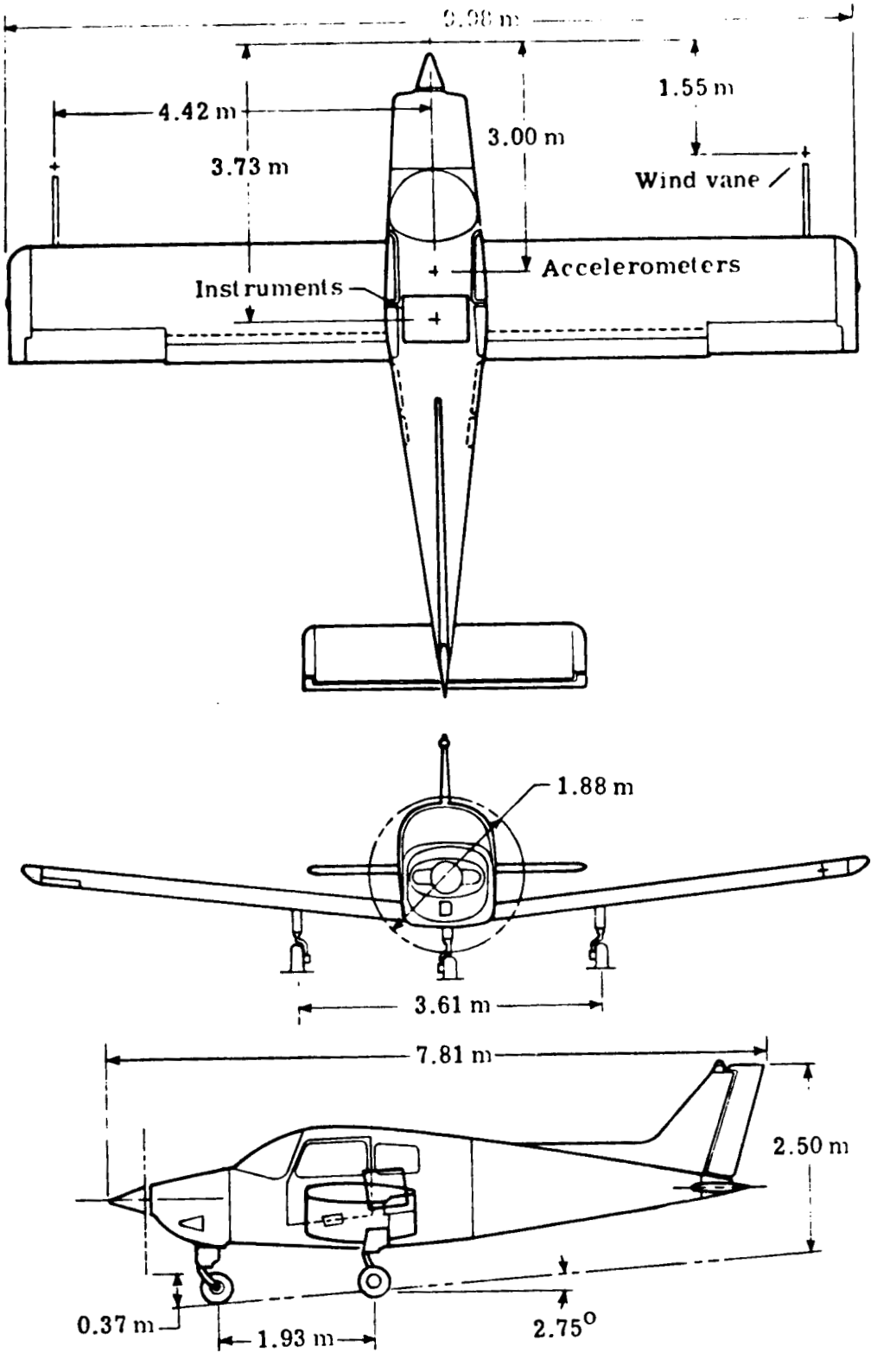

Figure 2.- Three View Drawing of Test Aircraft

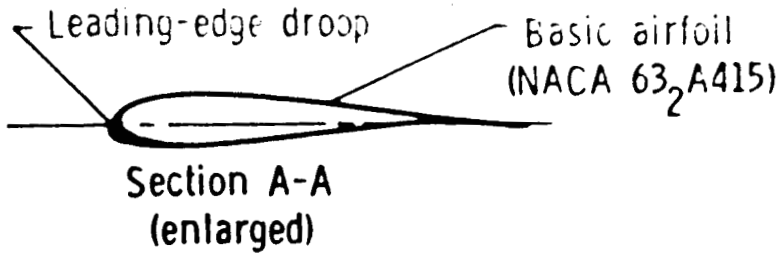

Section A-A
(enlarged)

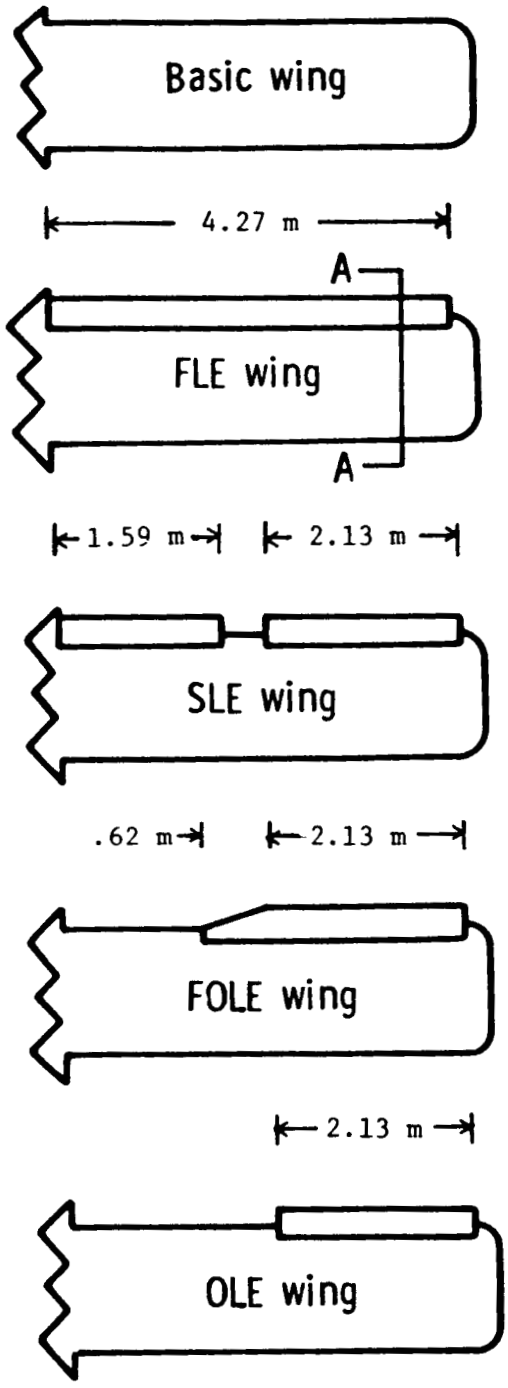

Figure 3.- Basic and Modified Wing Geometries

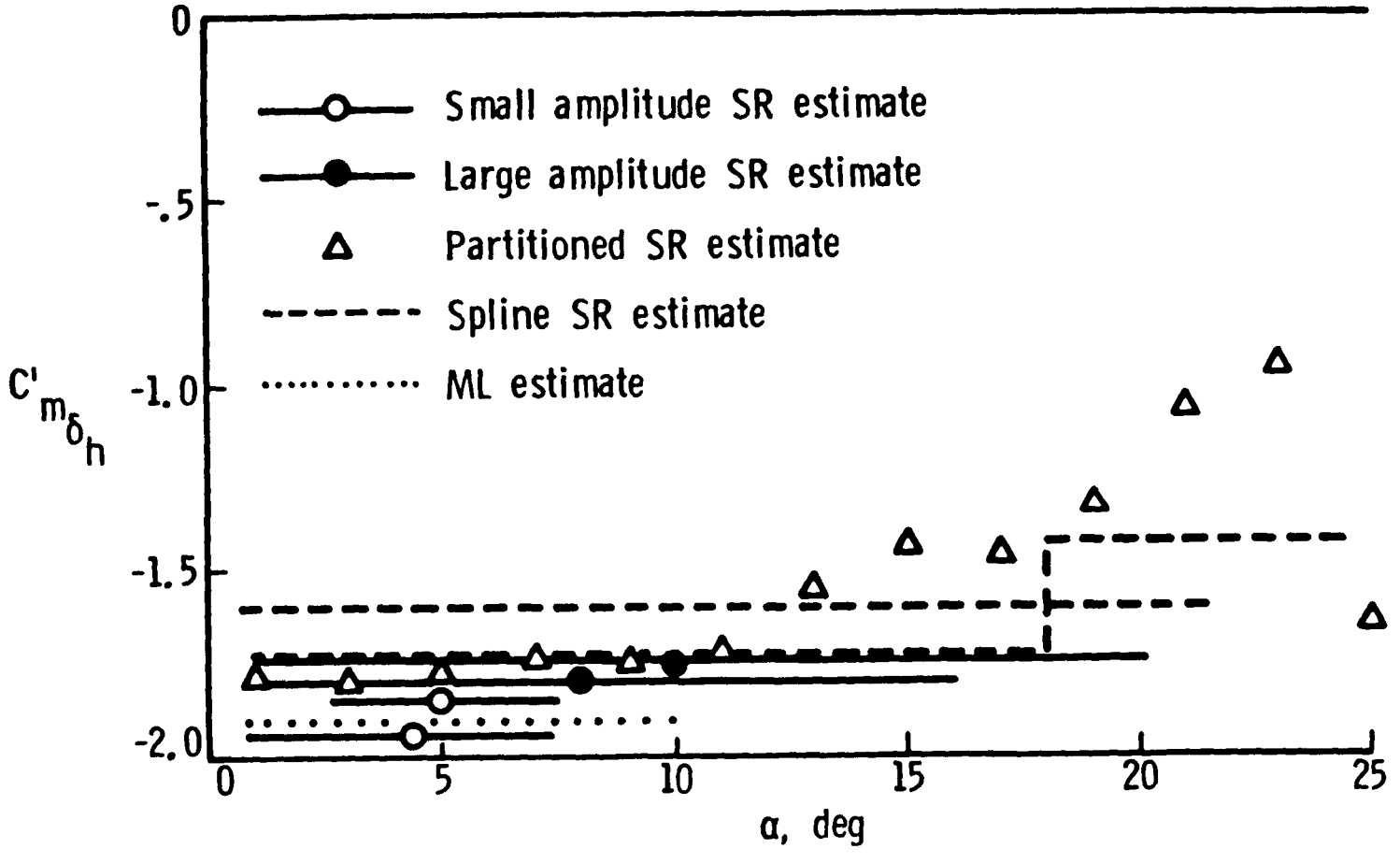

Figure 4.- SR and ML Estimates of $C'_{m_{\delta_h}}$ Parameter for the SLE Wing Configuration

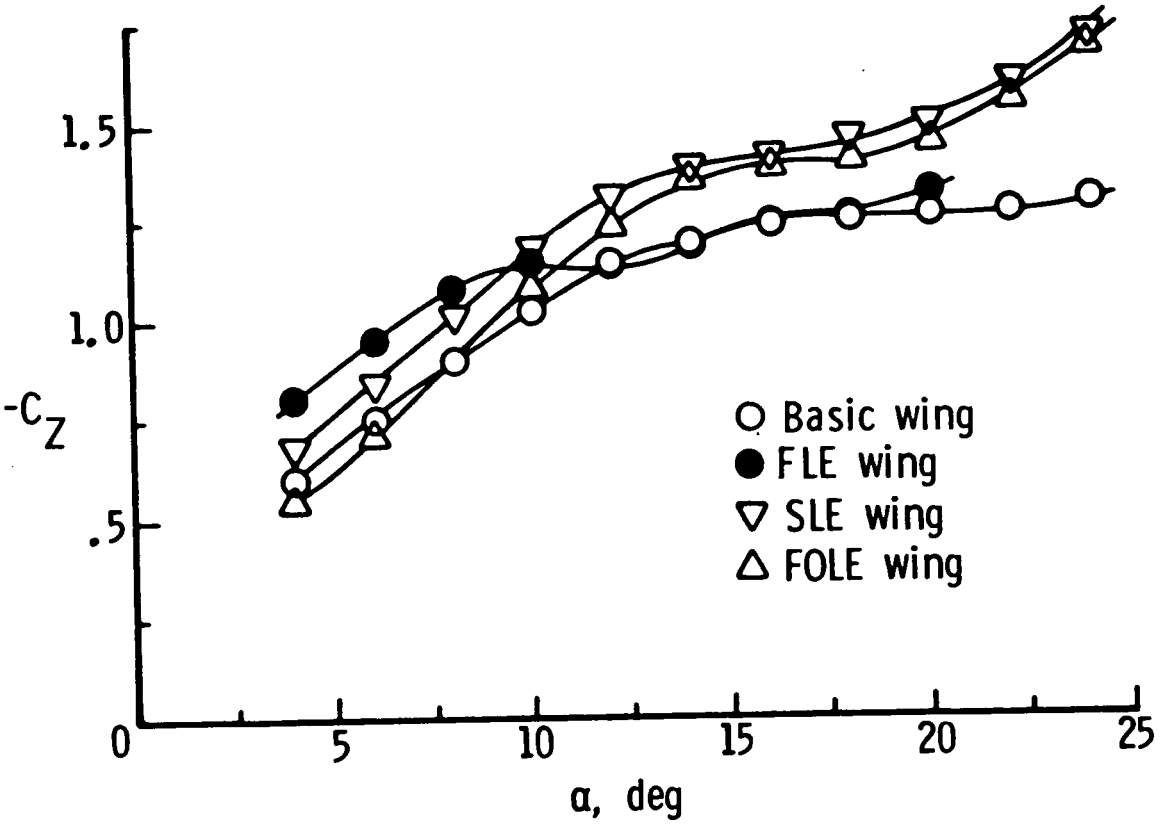

Figure 5.- Vertical Force Parameter Estimates

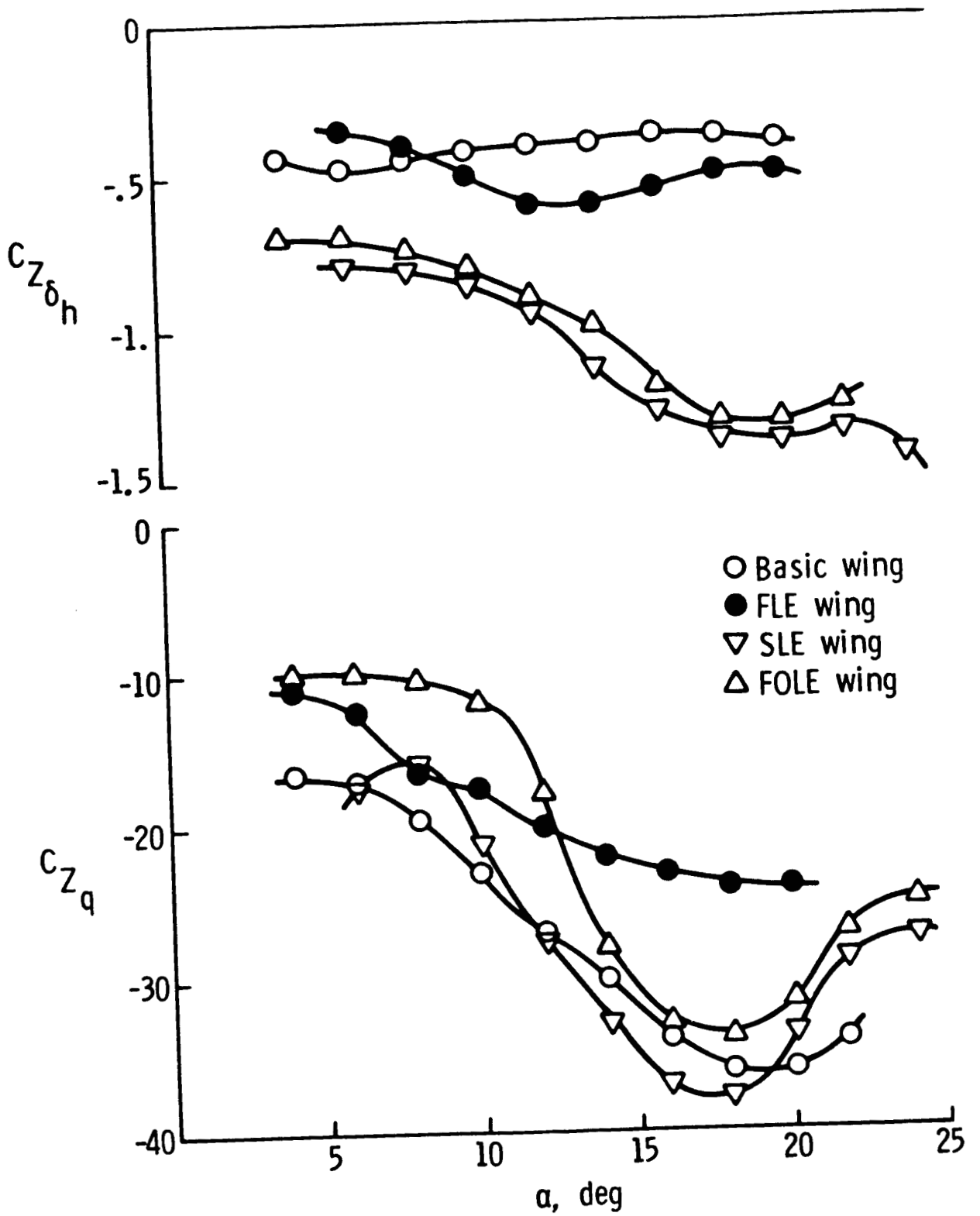

Figure 5.- Concluded

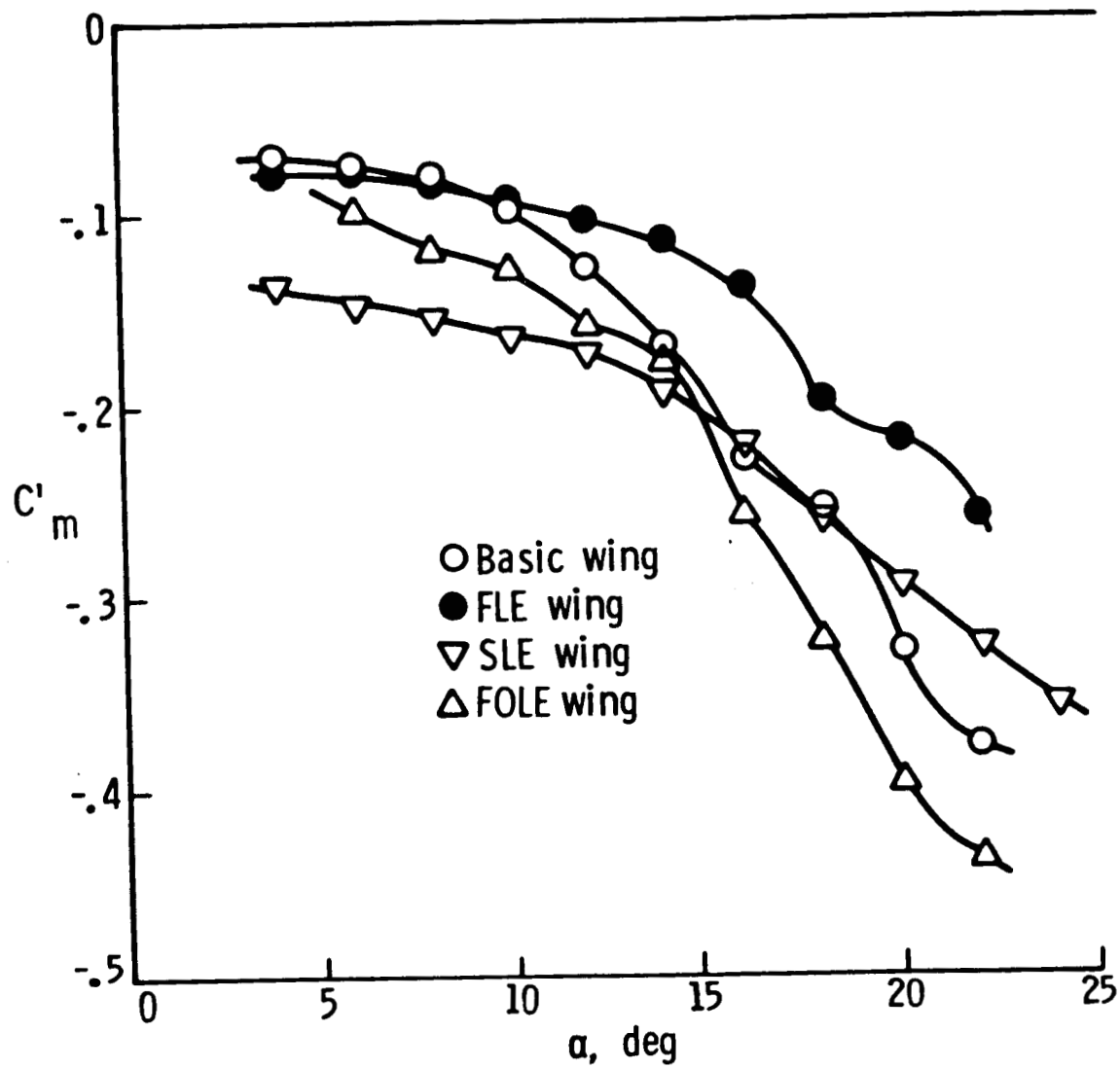

Figure 6.- Pitching Moment Parameter Estimates

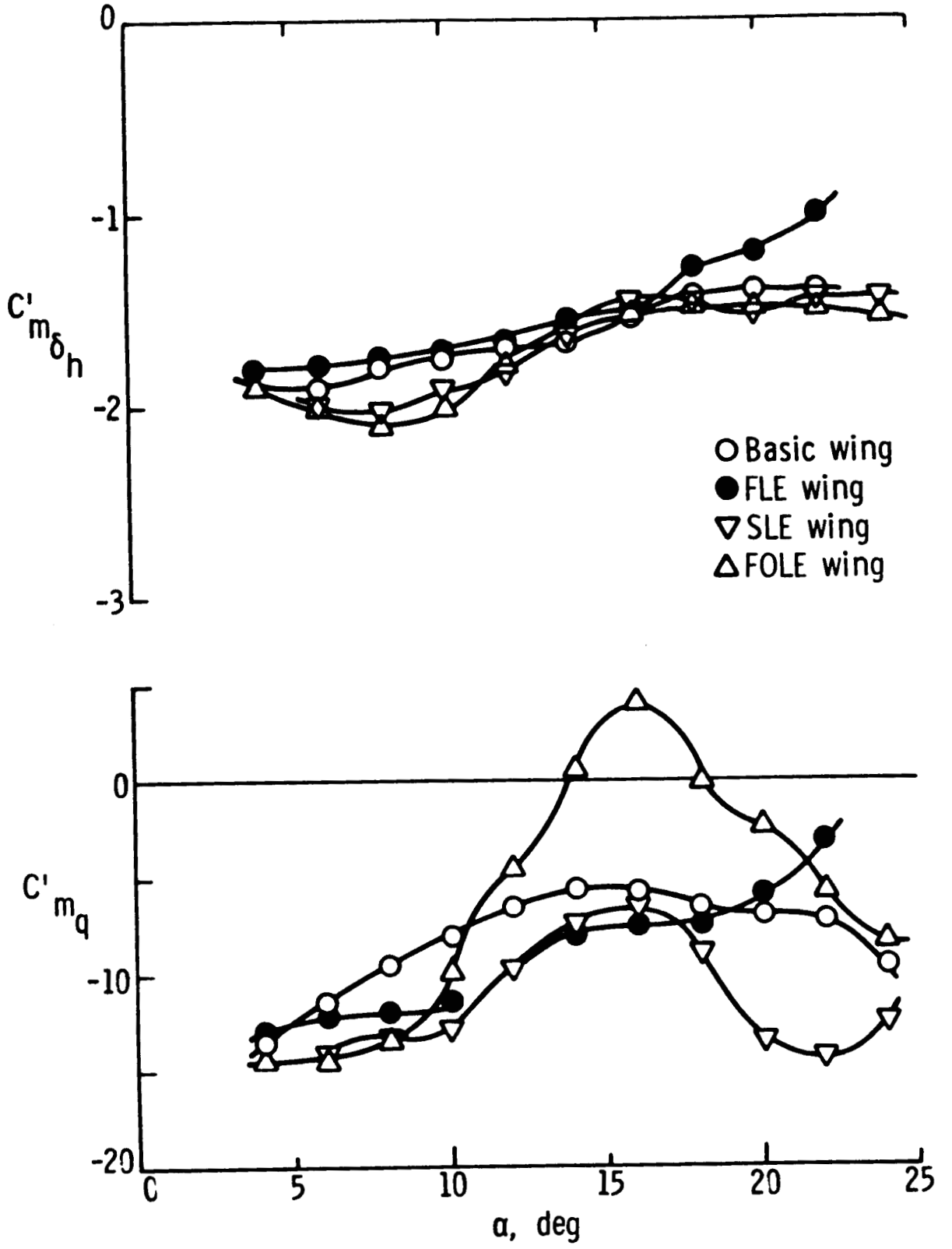

Figure 6.- Concluded

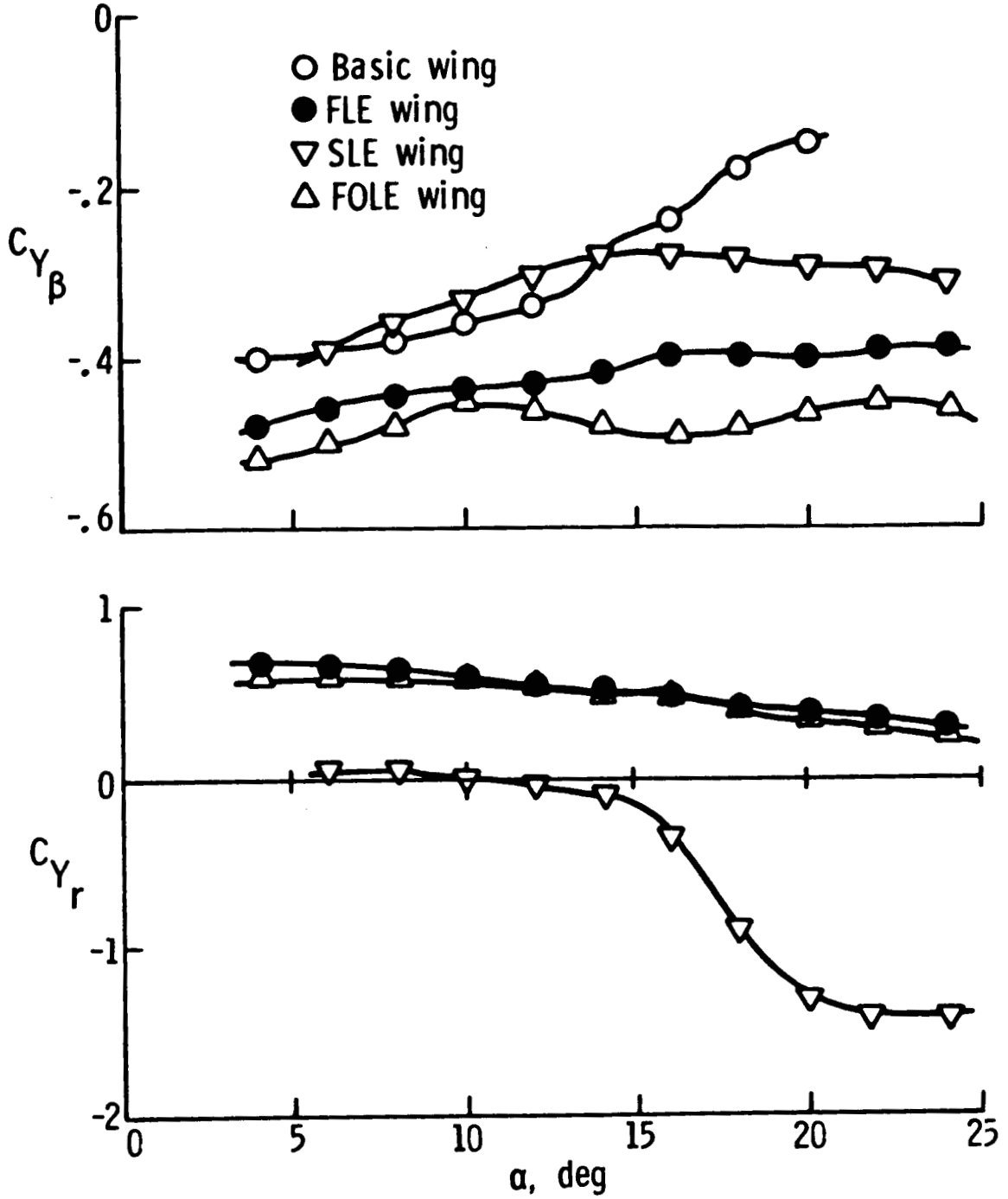

Figure 7.- Lateral Force Parameter Estimates

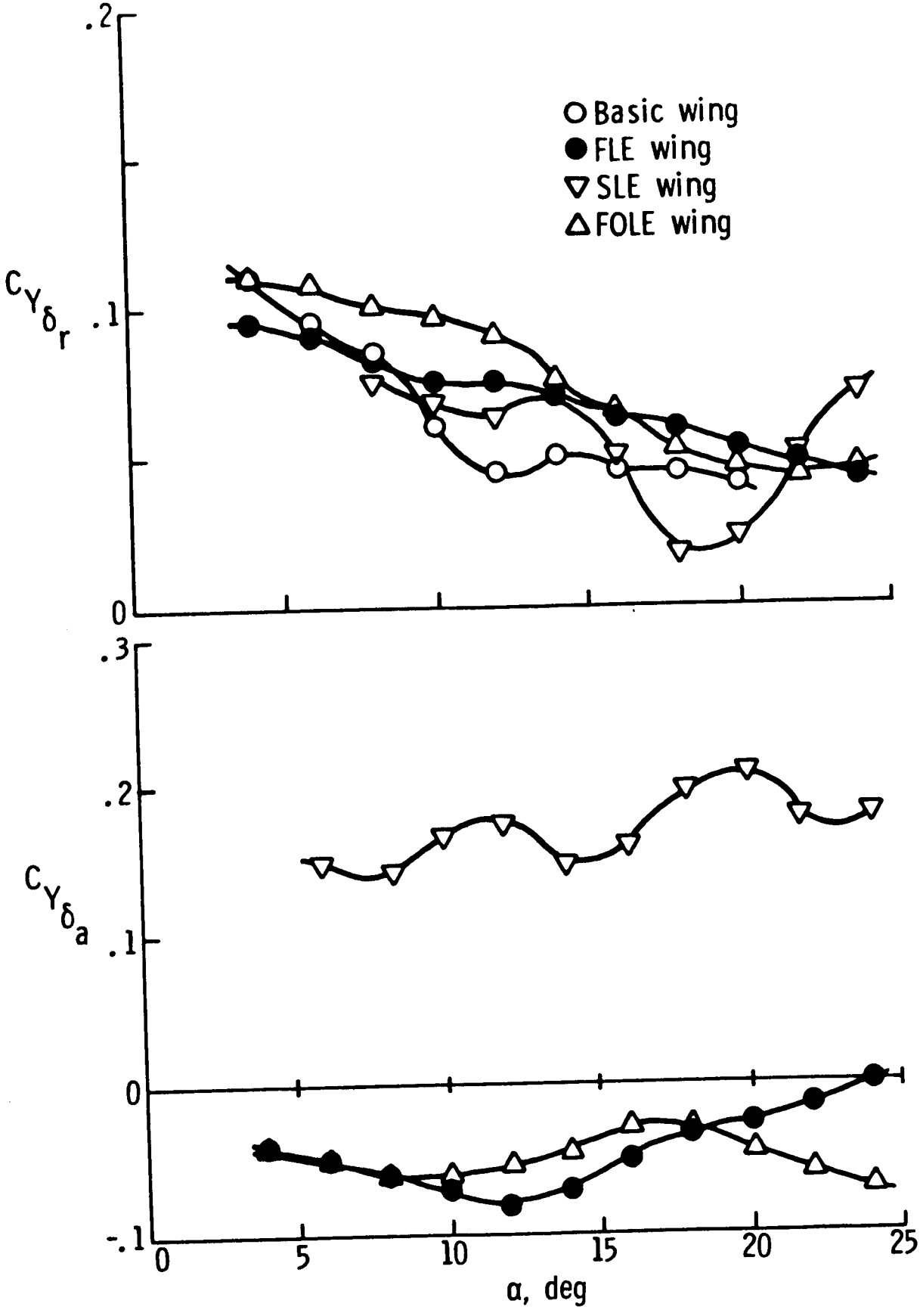

Figure 7.- Concluded

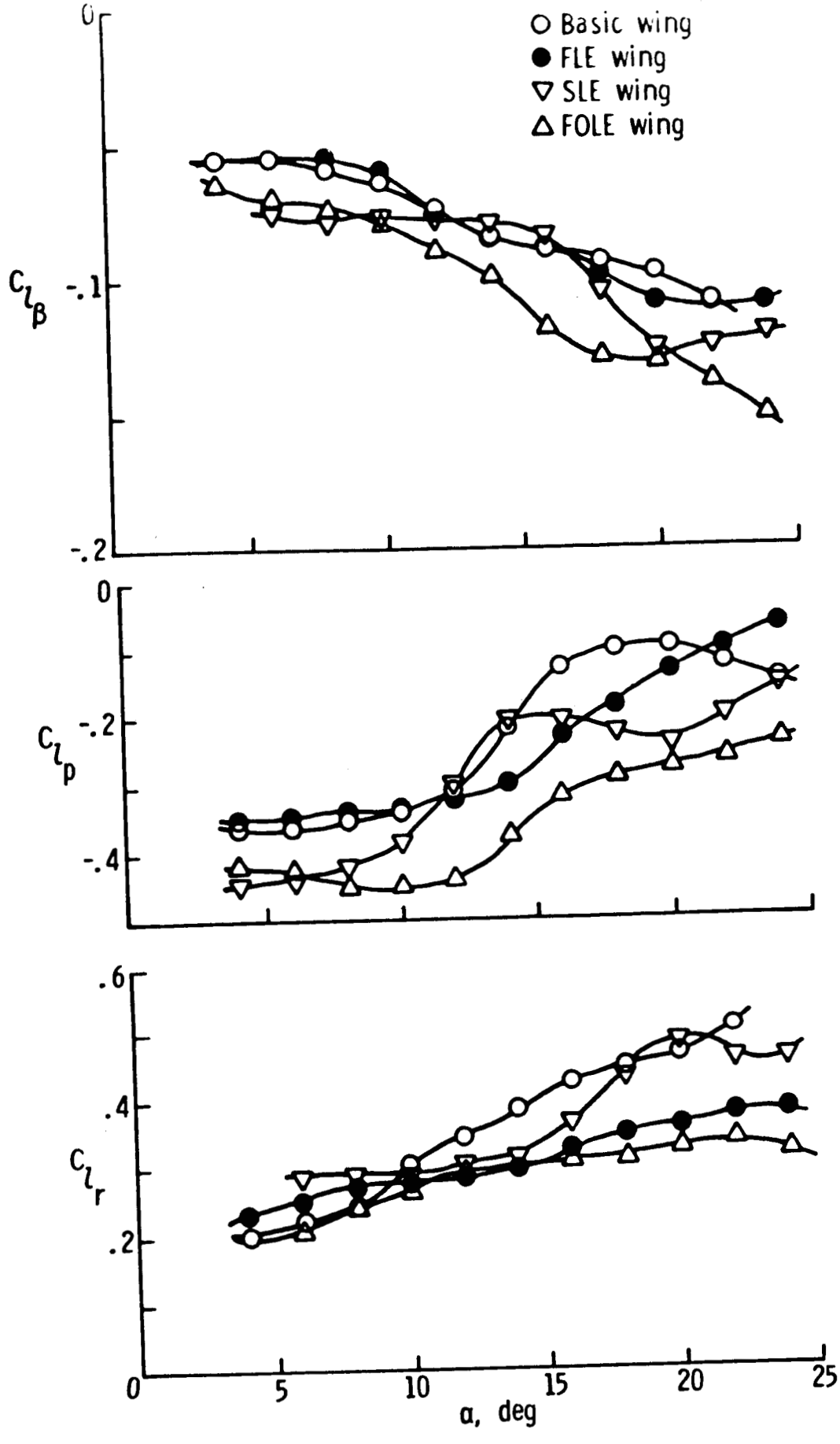

Figure 8.- Rolling Moment Parameter Estimates

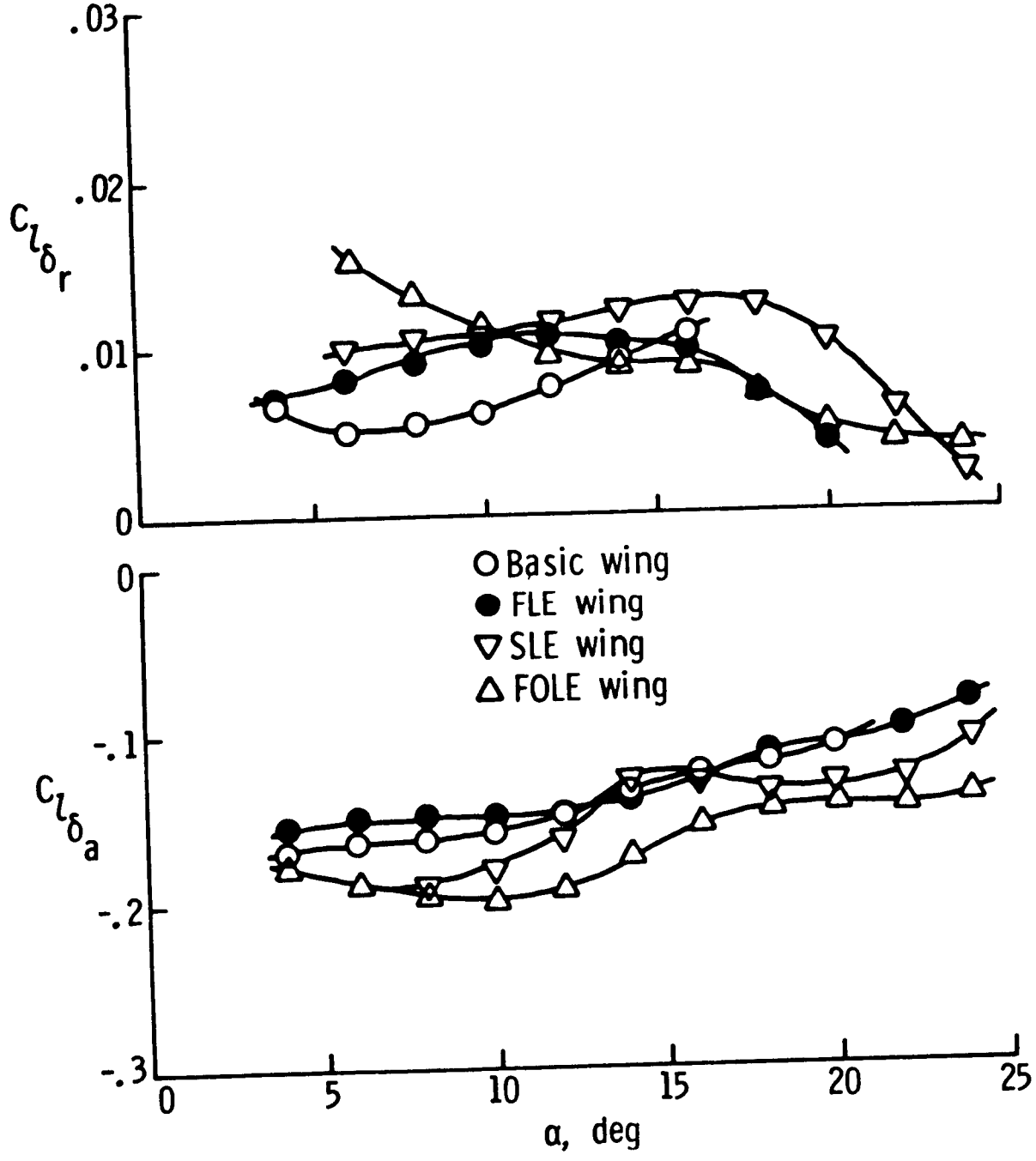

Figure 8.- Concluded

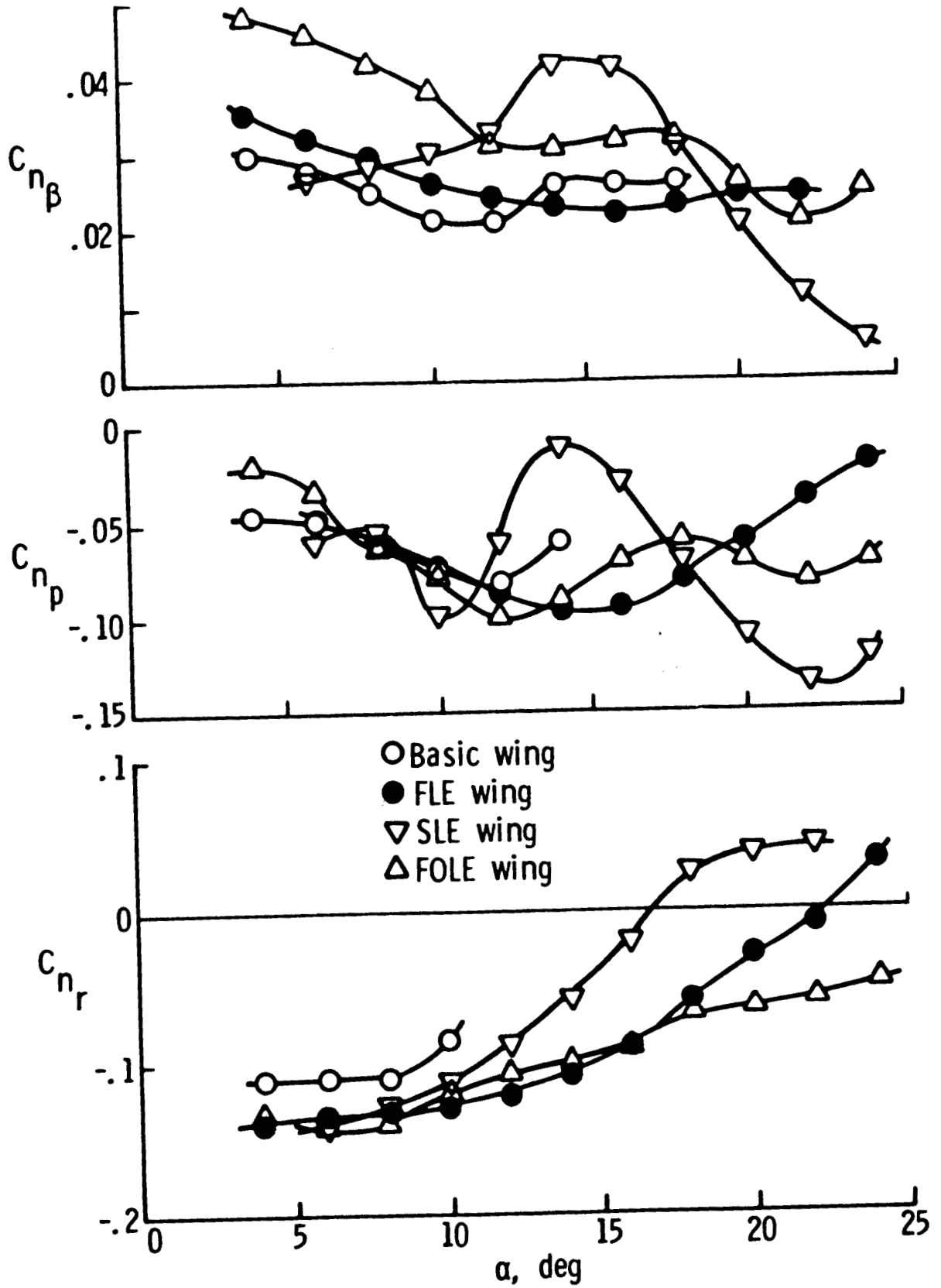

Figure 9.- Yawing Moment Parameter Estimates

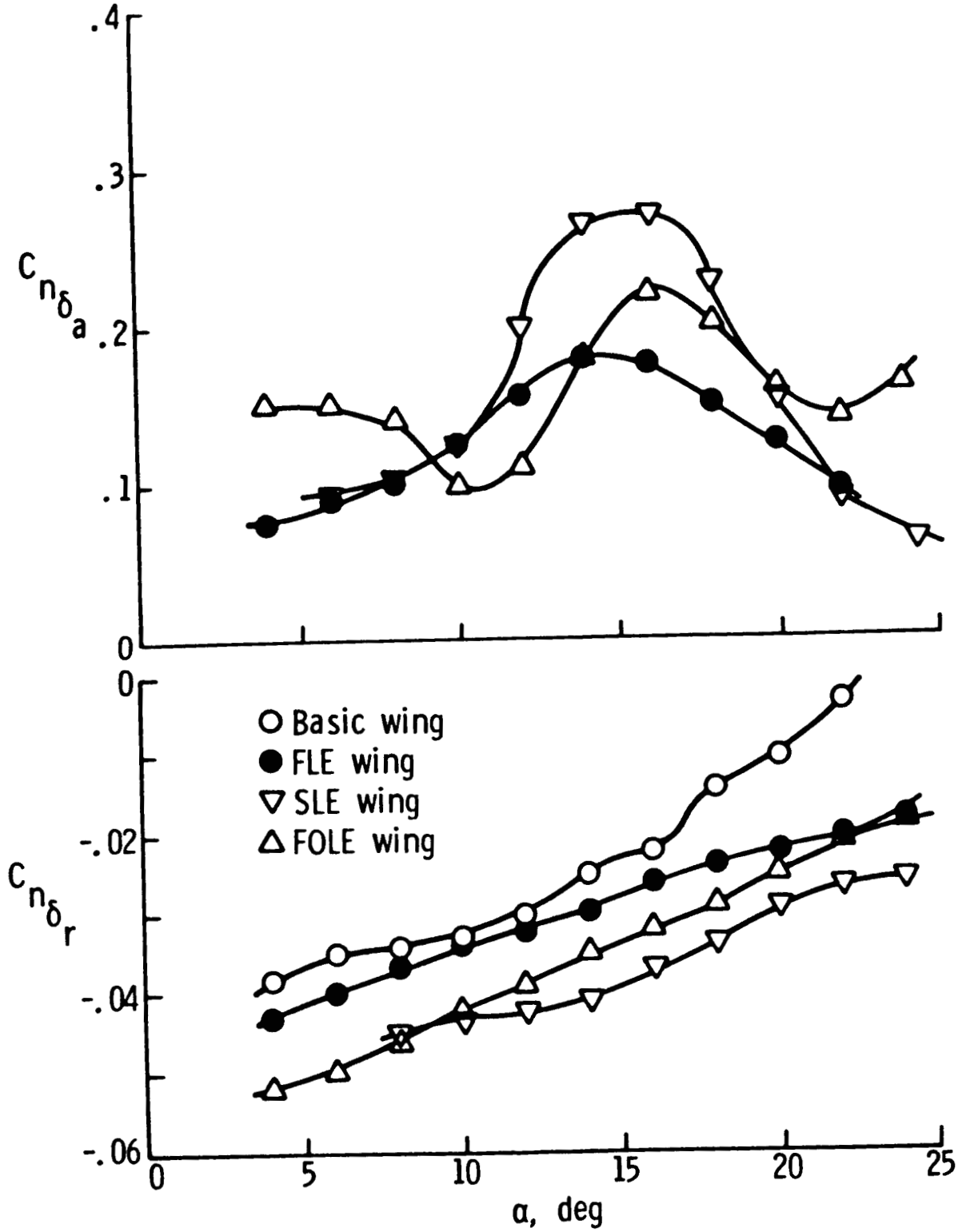

Figure 9.- Concluded

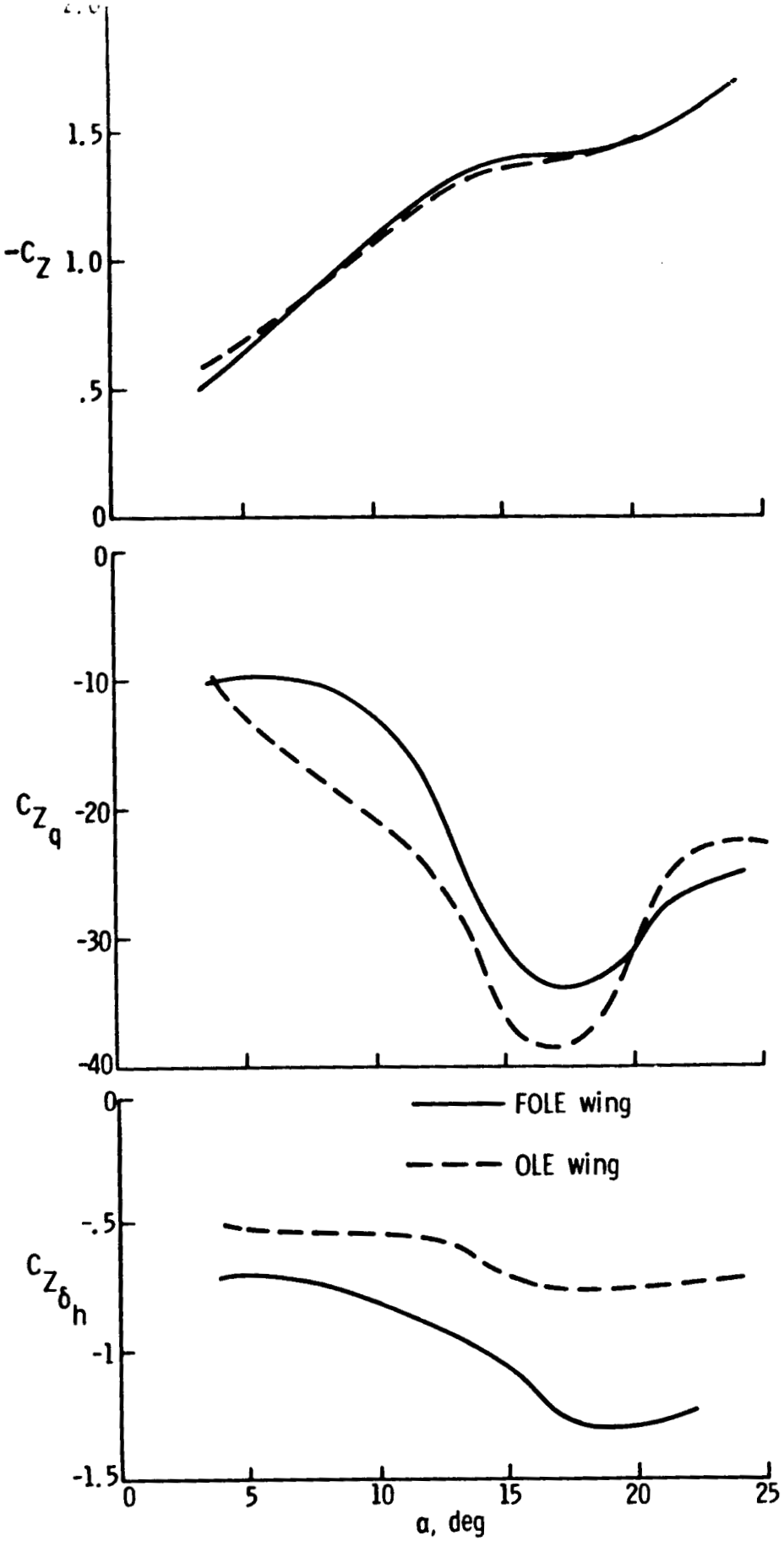

Figure 10.- Comparison Between OLE and FOLE Geometry Parameter Estimates

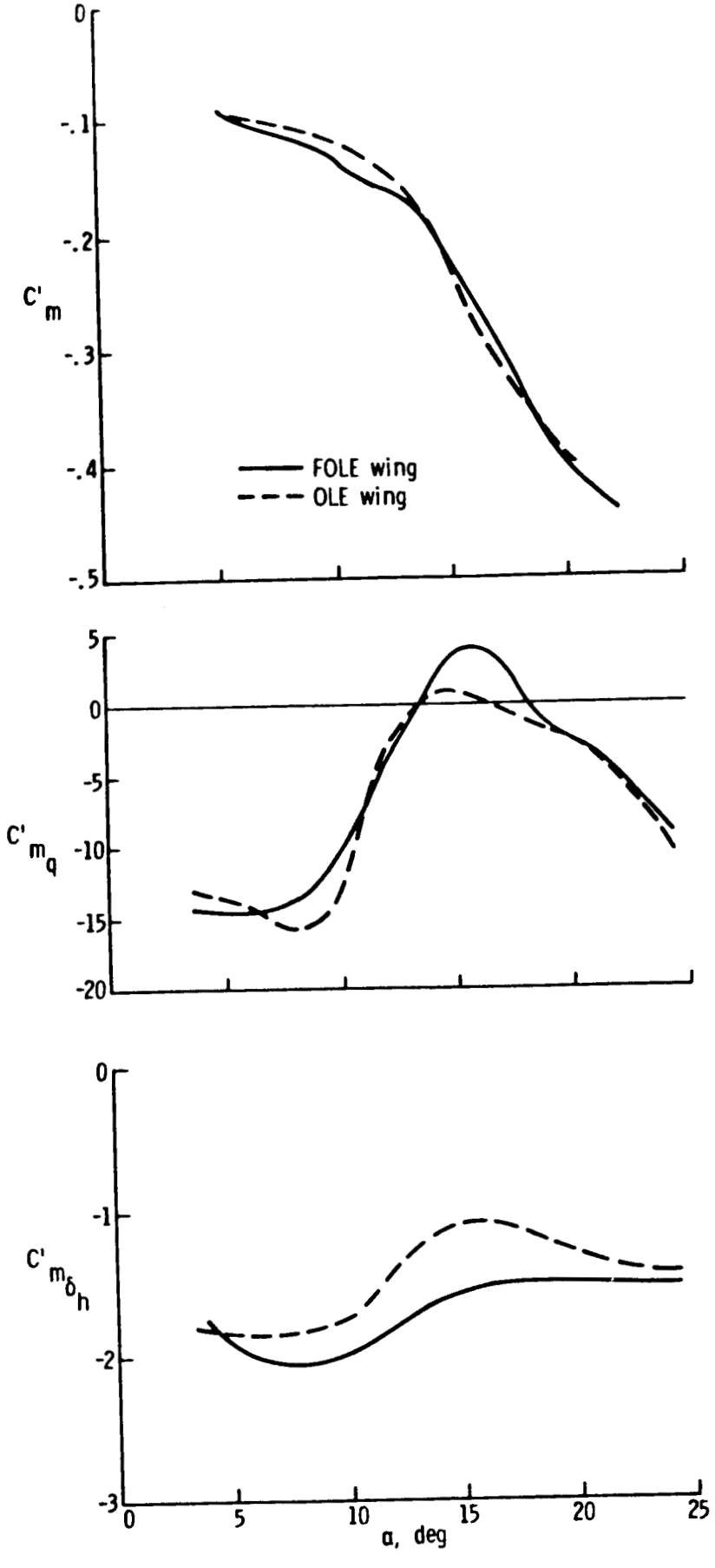

Figure 10.- Continued

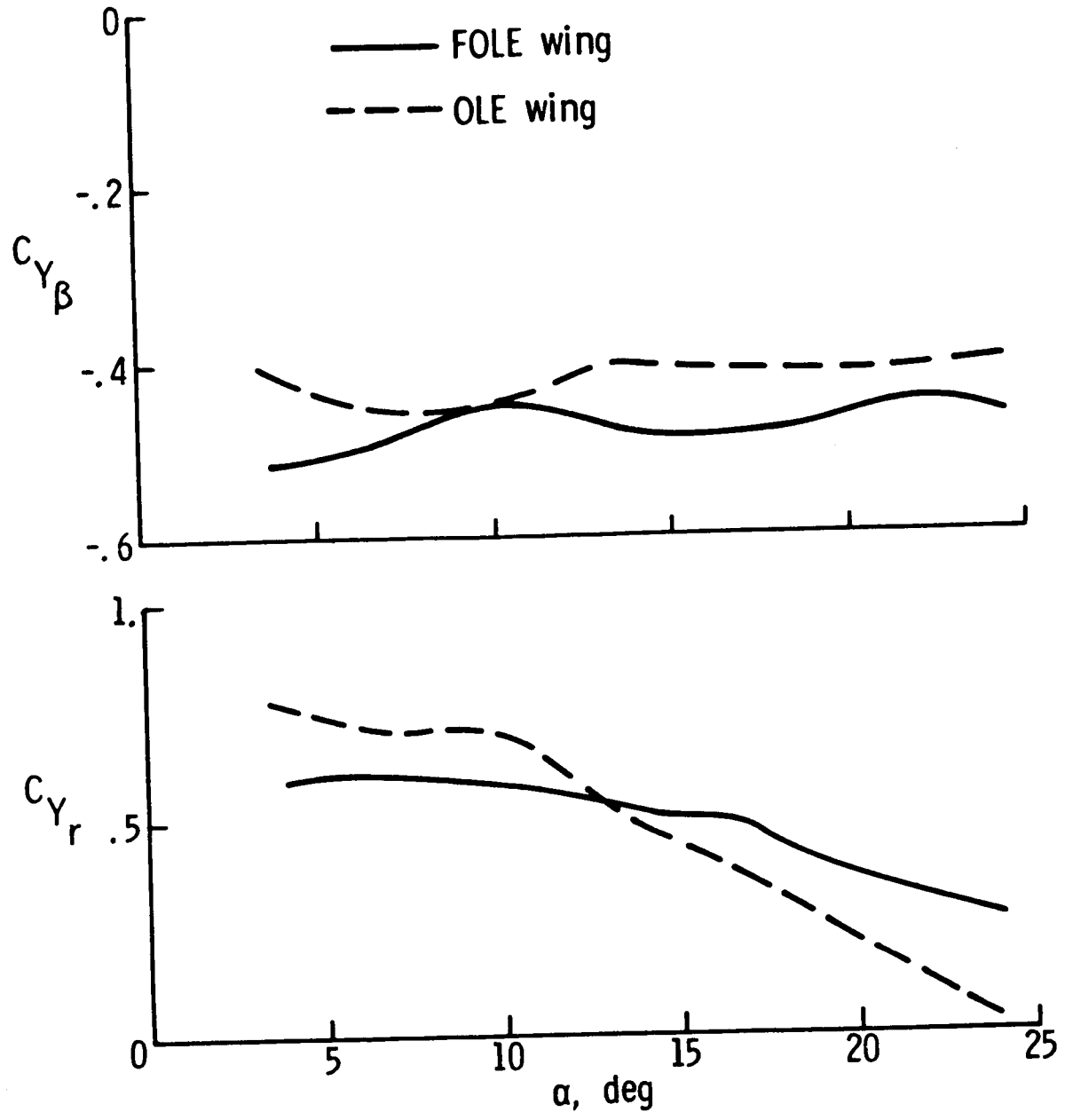

Figure 10.- Continued

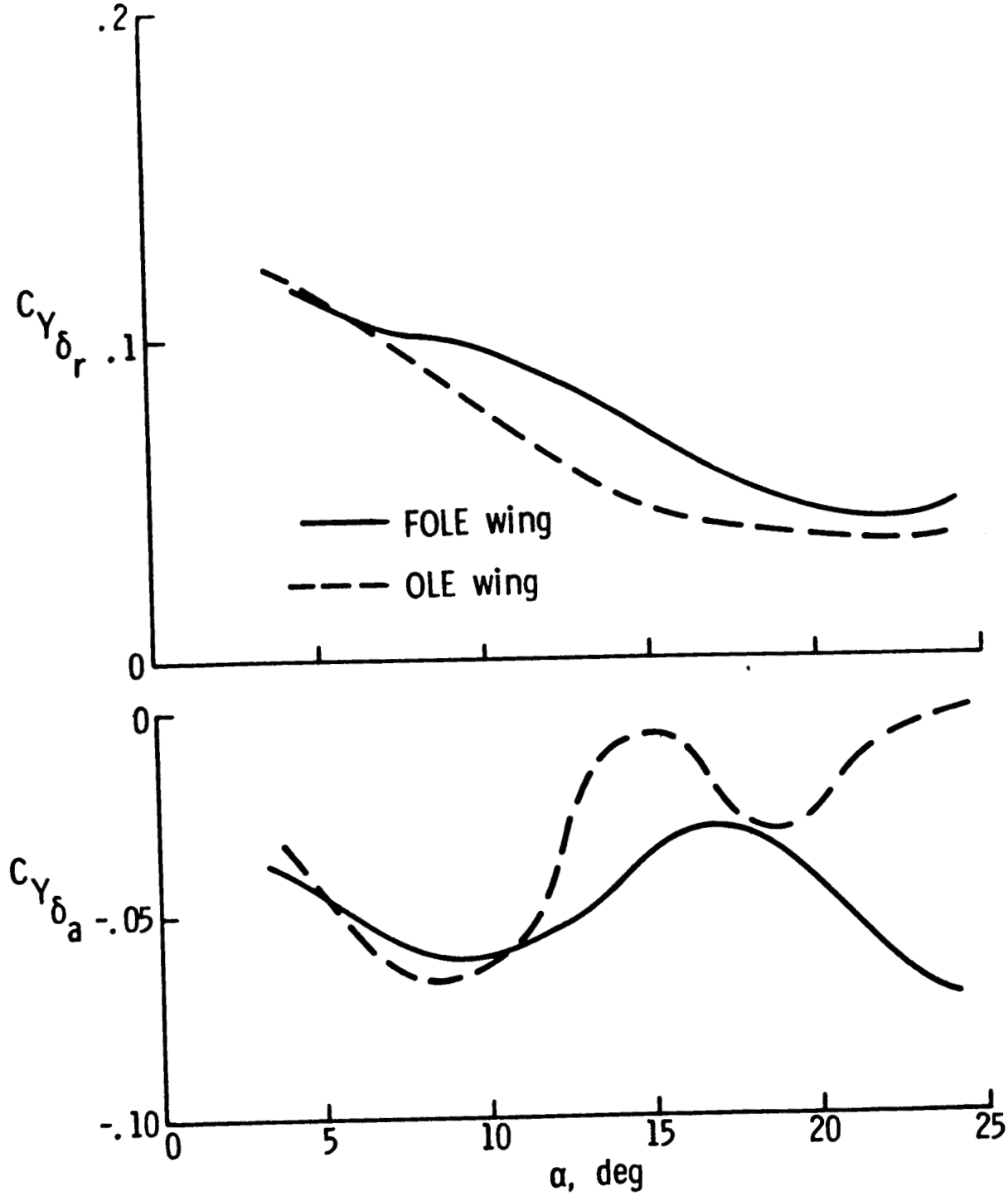

Figure 10.- Continued

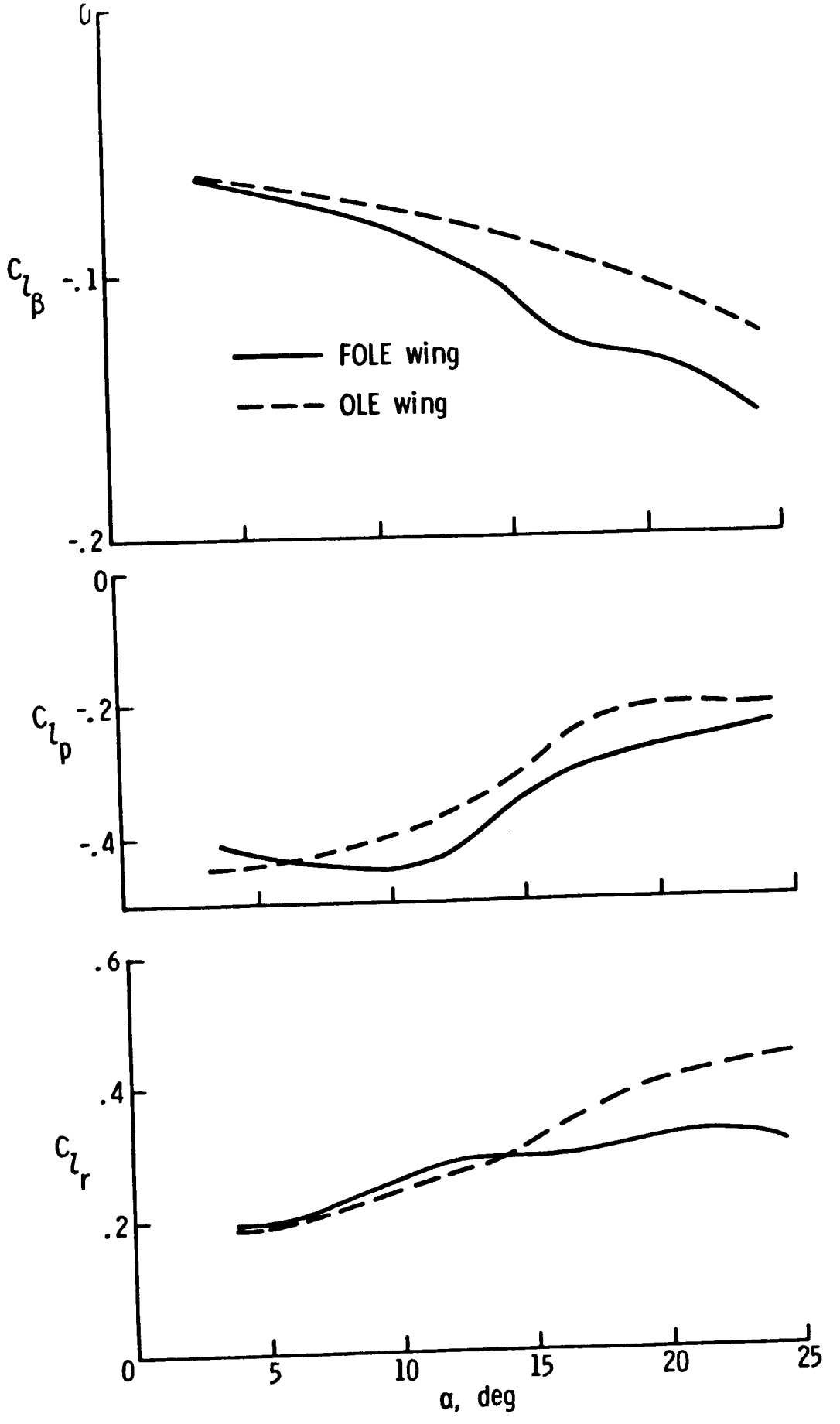

Figure 10.- Continued

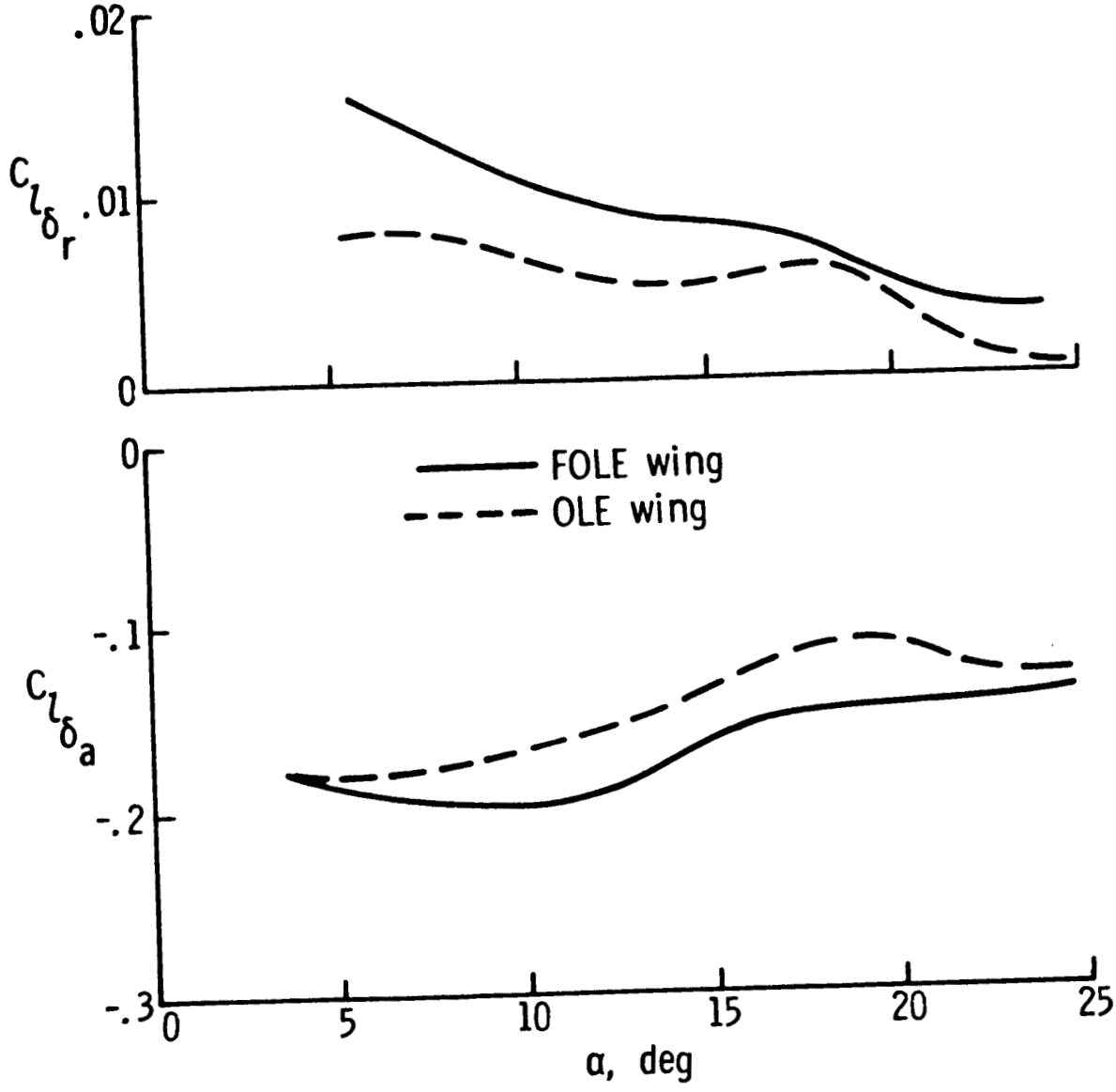

Figure 10.- Continued

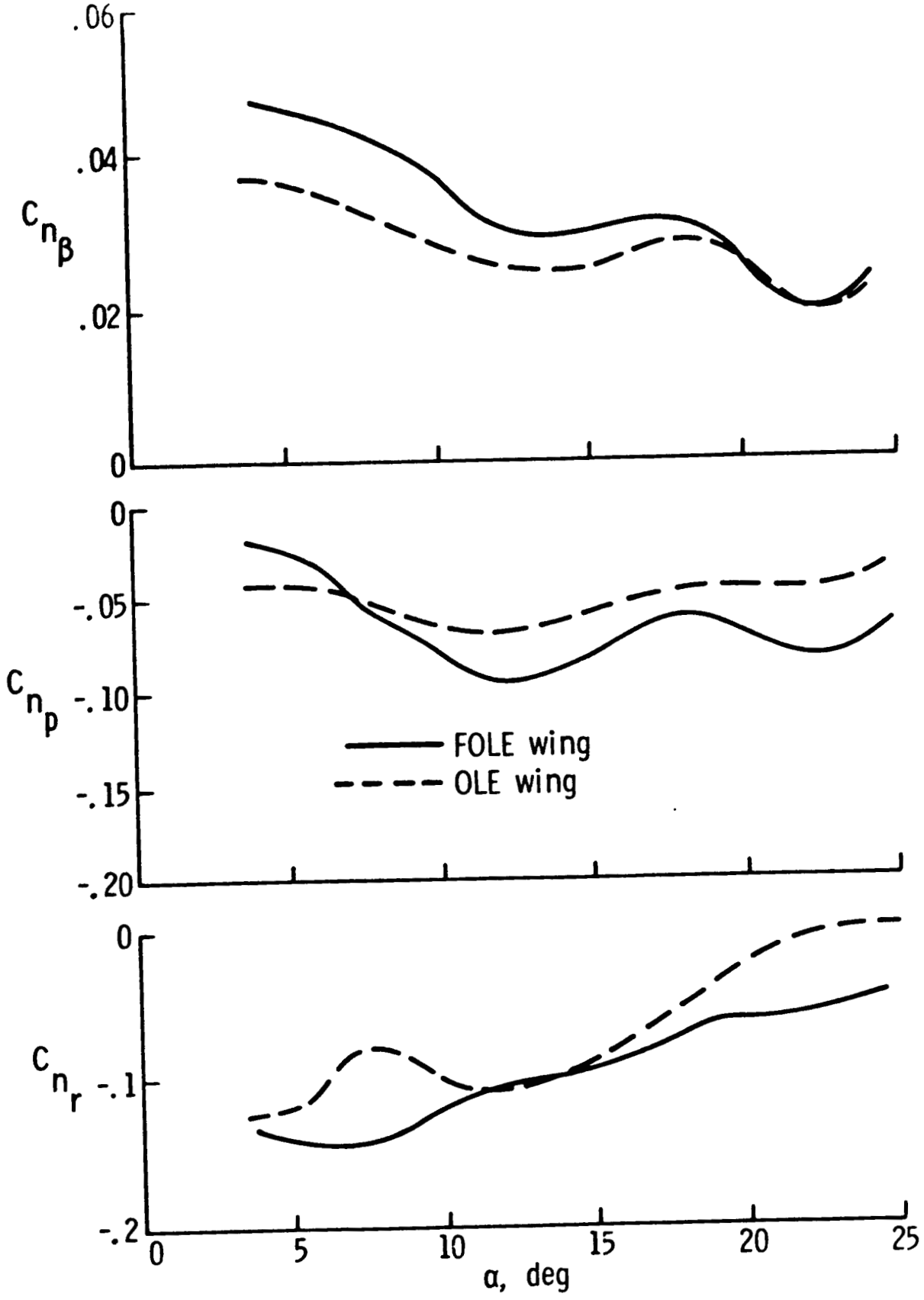

Figure 10.- Continued

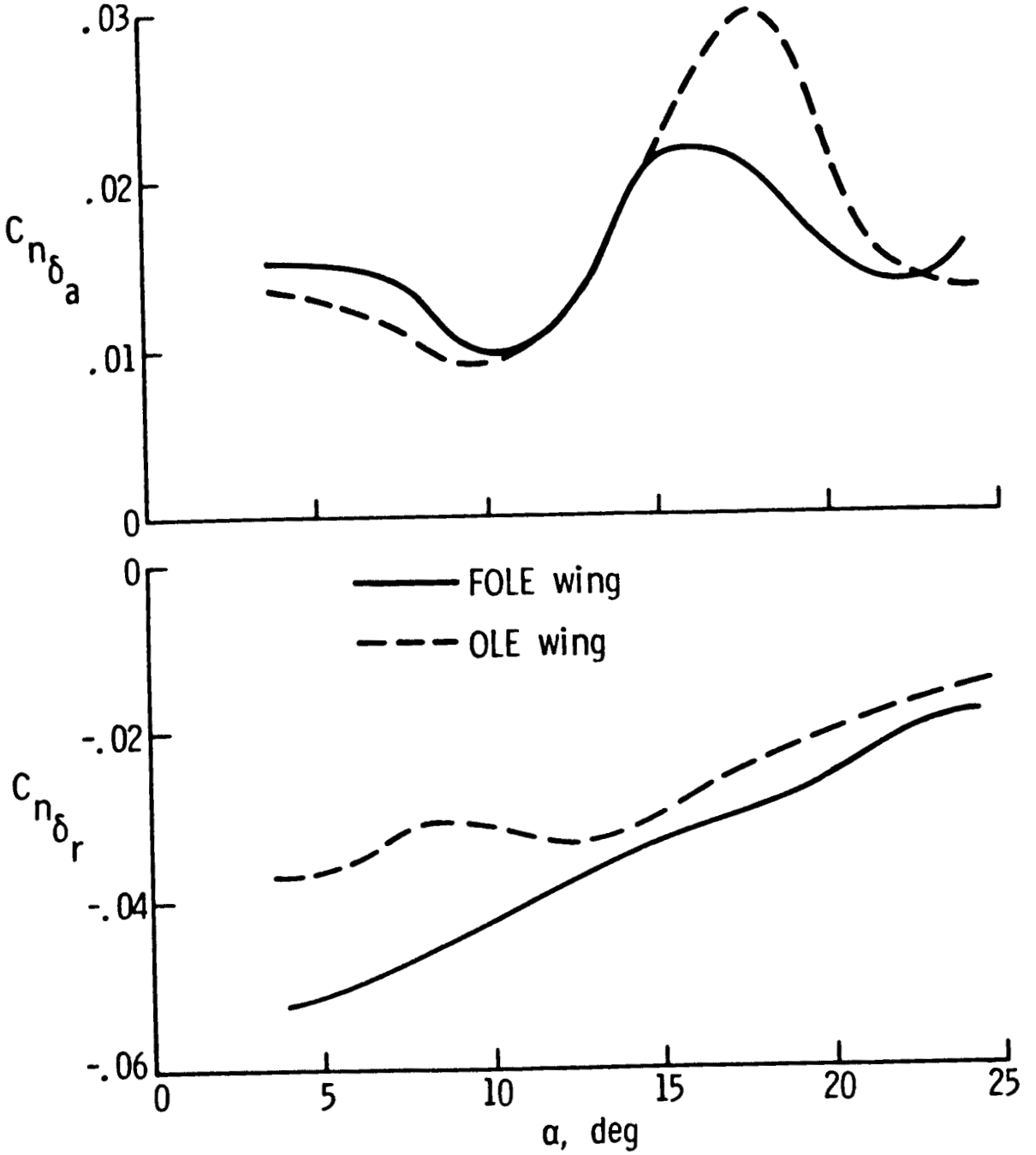

Figure 10.- Concluded

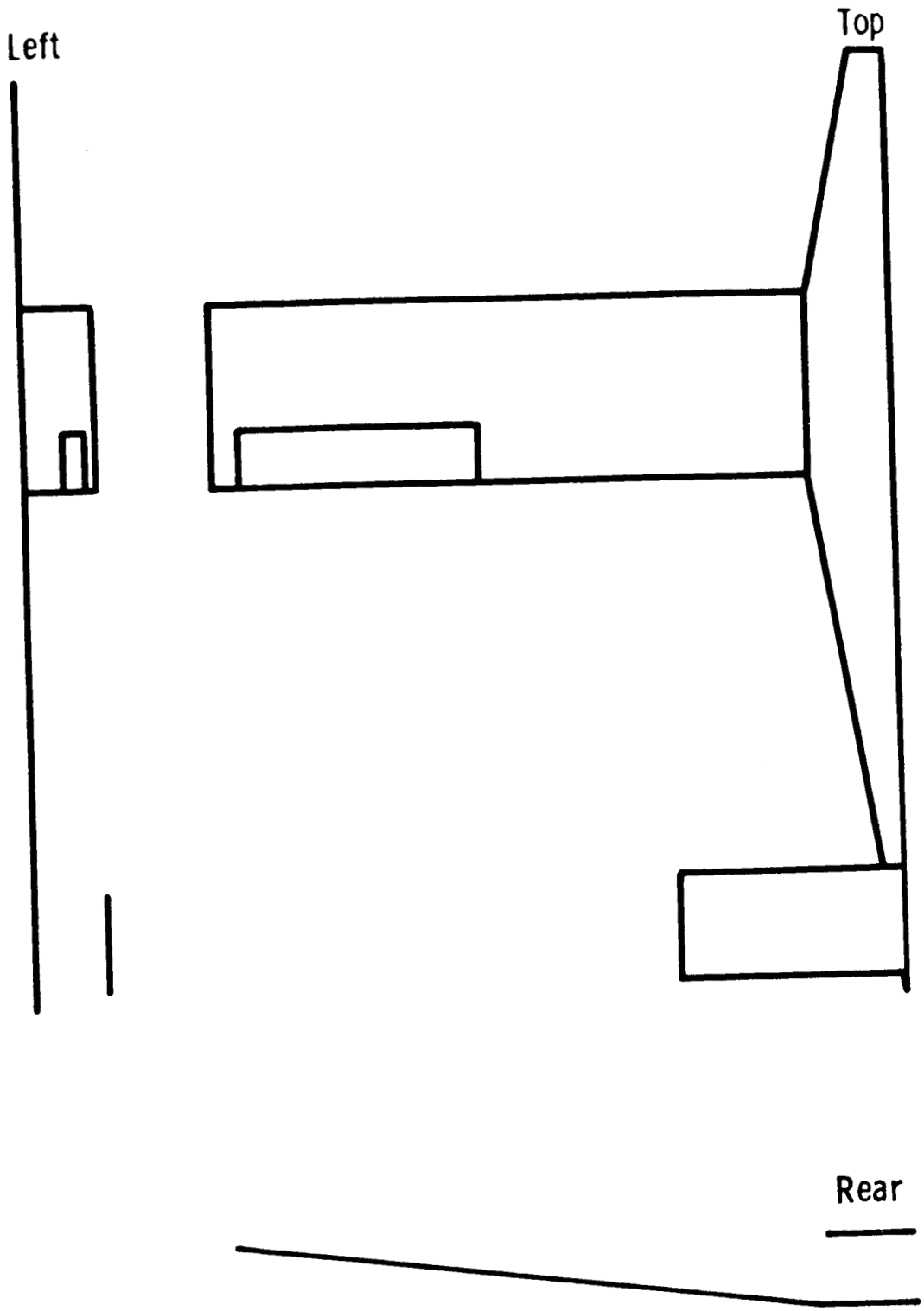

Figure 11a.- Longitudinal VL Planform

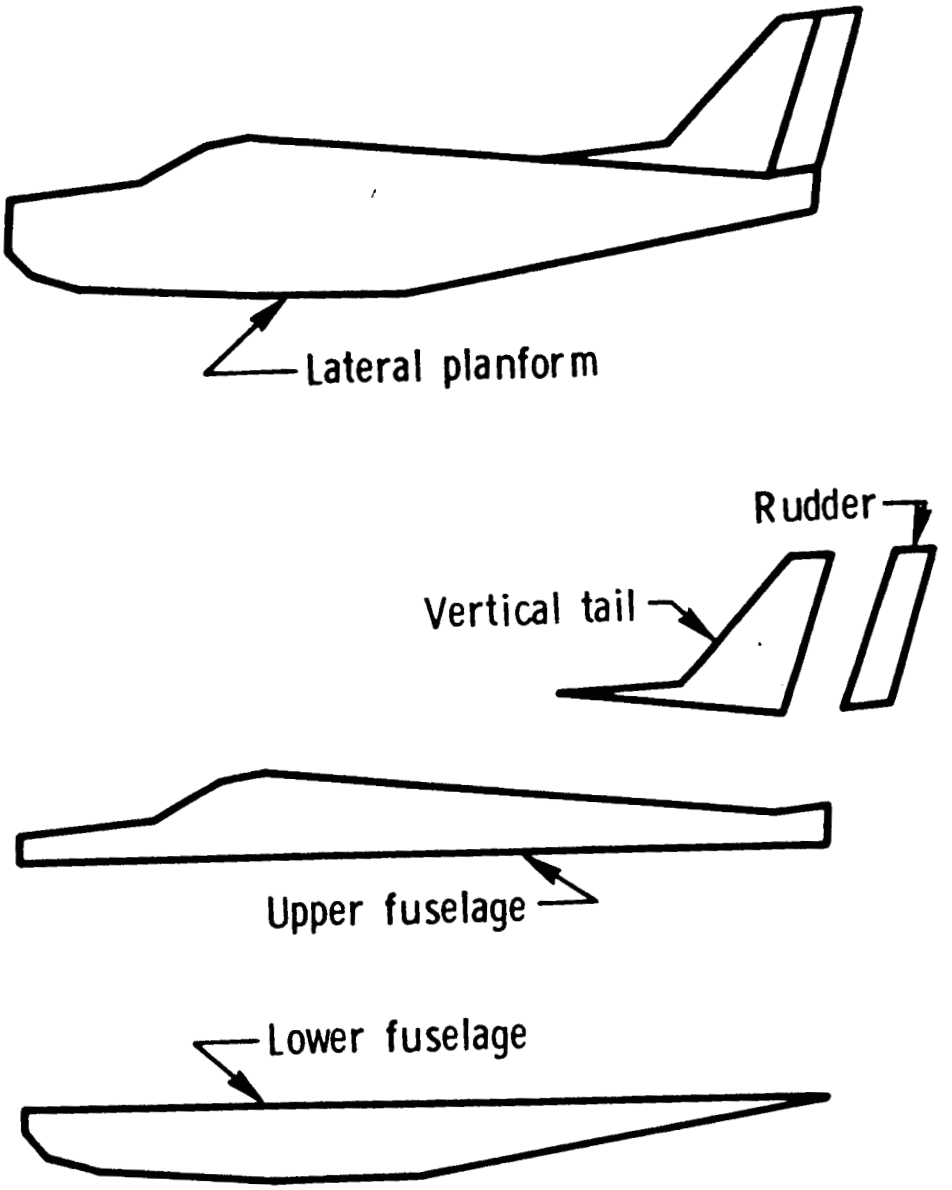

Figure 11b.- Lateral VL Planform

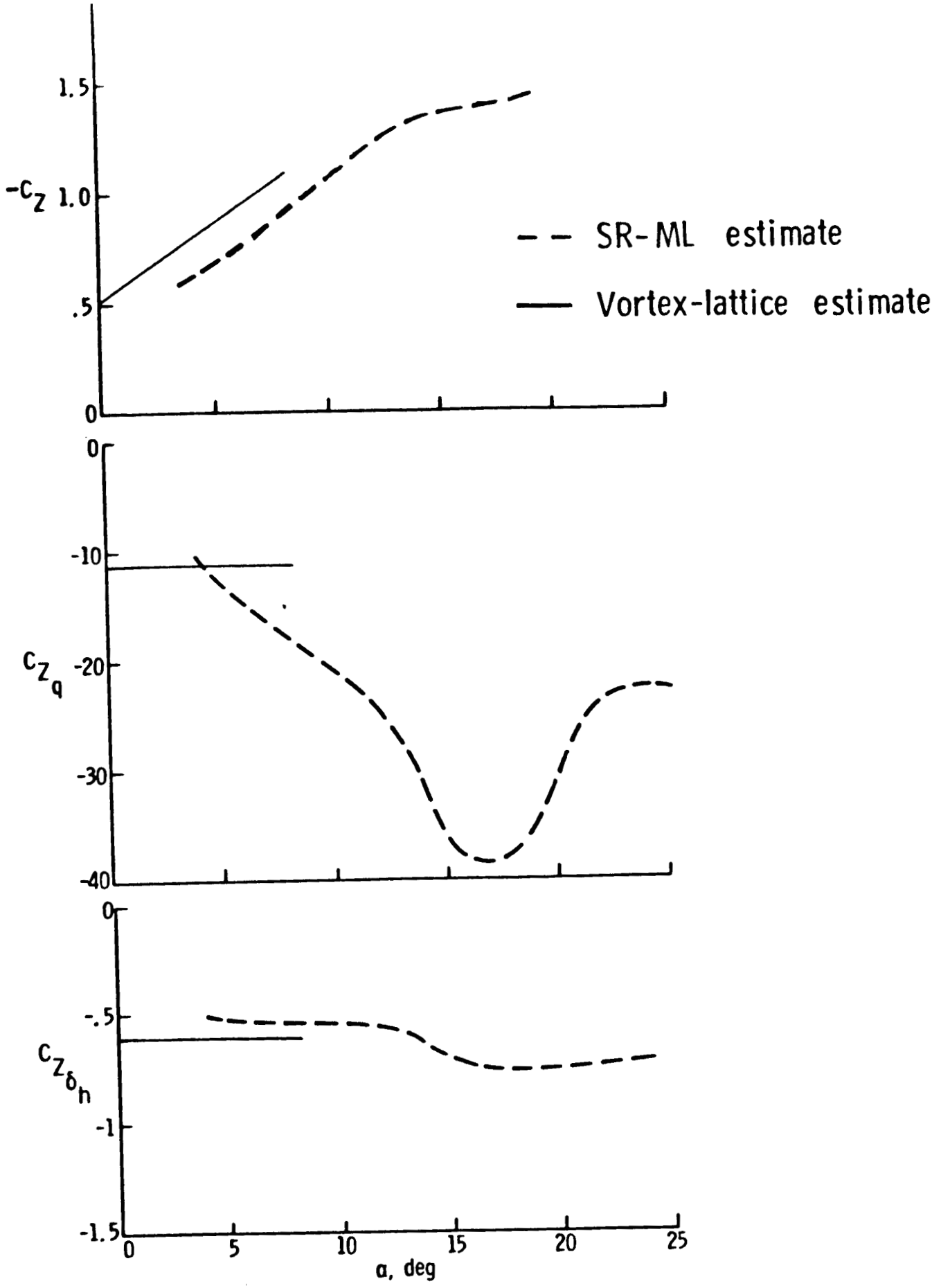

Figure 12a.- Comparison of Theoretical and Estimated Parameters for the OLE Wing Configuration

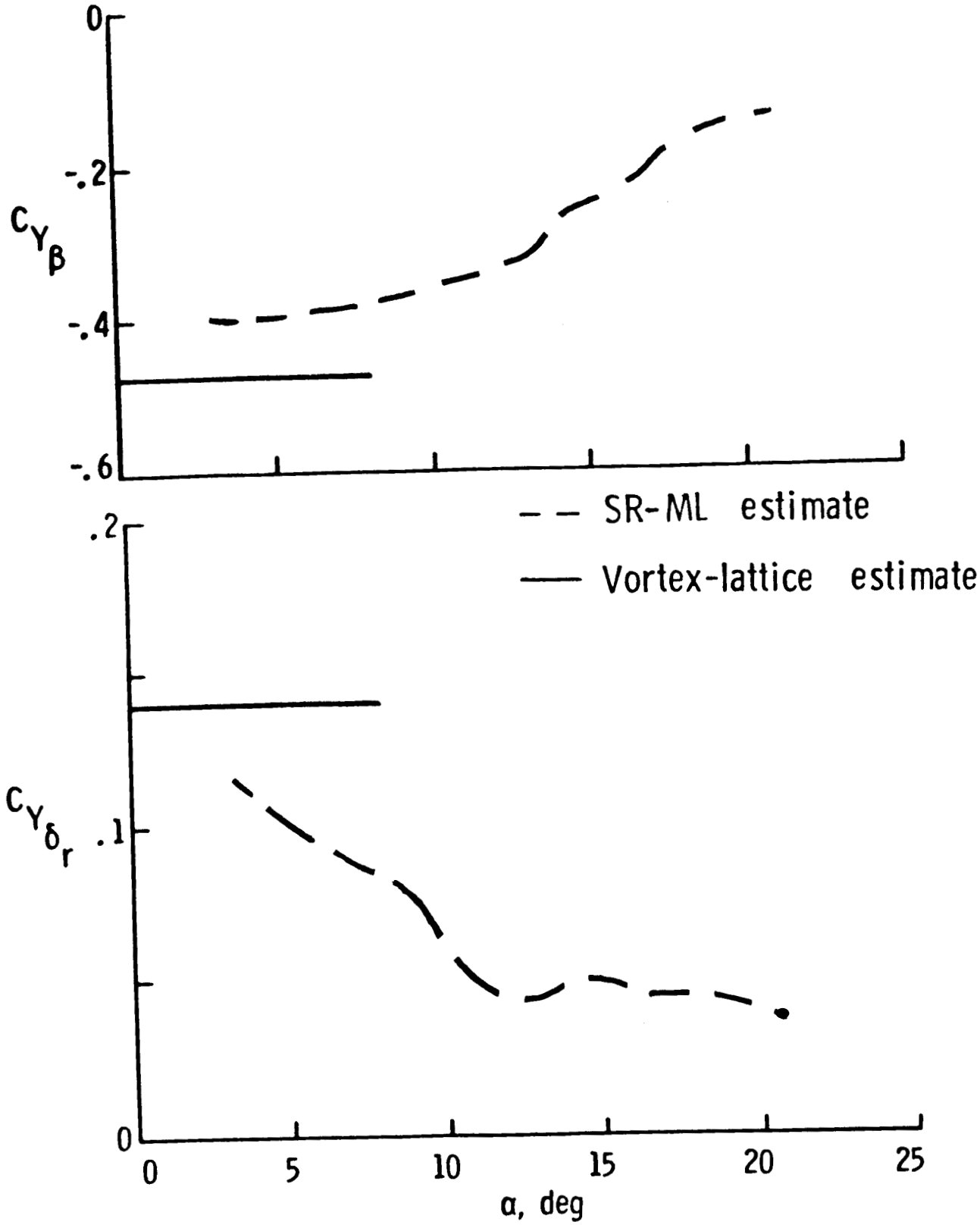

Figure 12b.- Comparison of Theoretical and Estimated Parameters for the Basic Wing Configuration

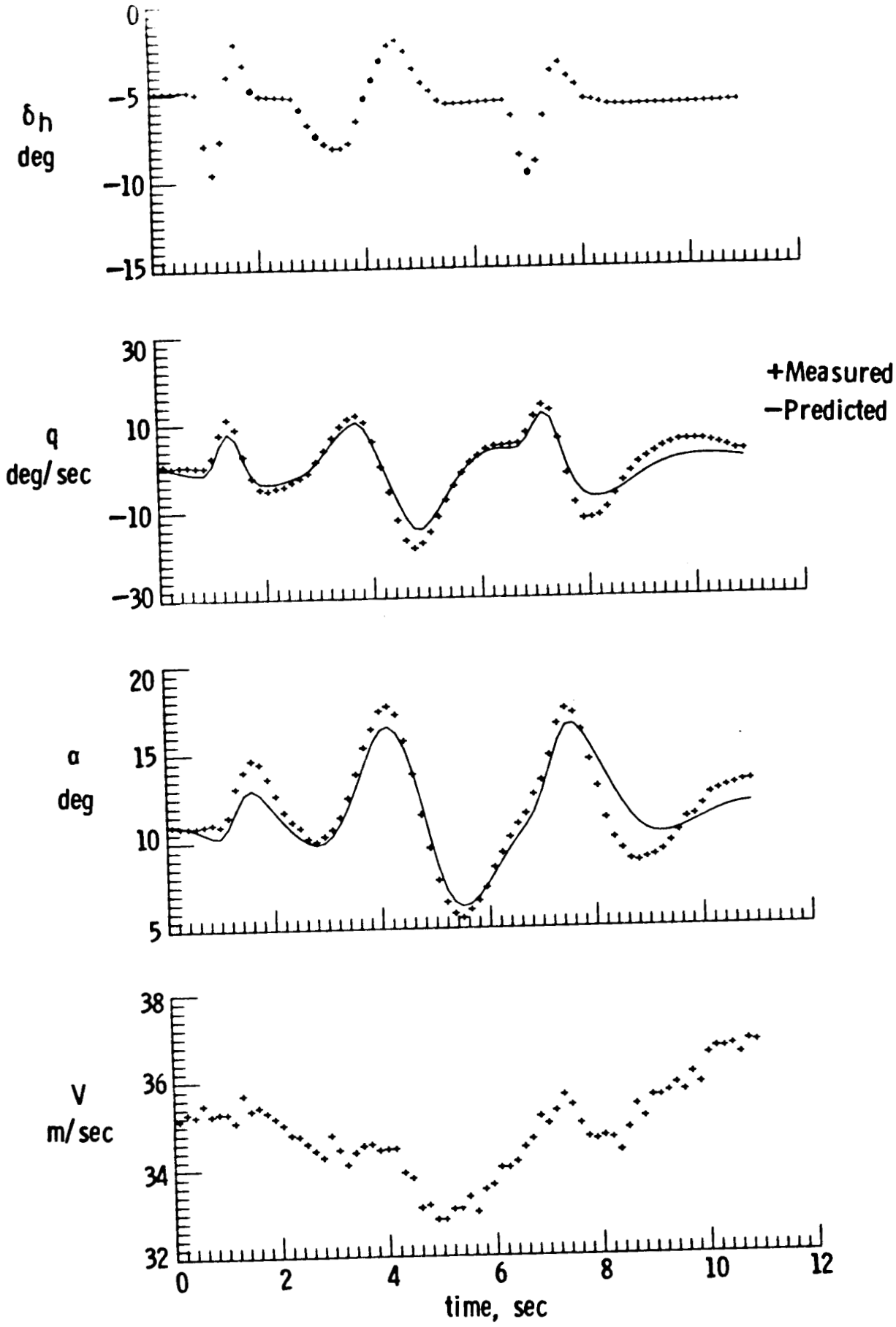

Figure 13a.- Comparison of Measured and Predicted Longitudinal Time Histories for FOLE Modified Wing

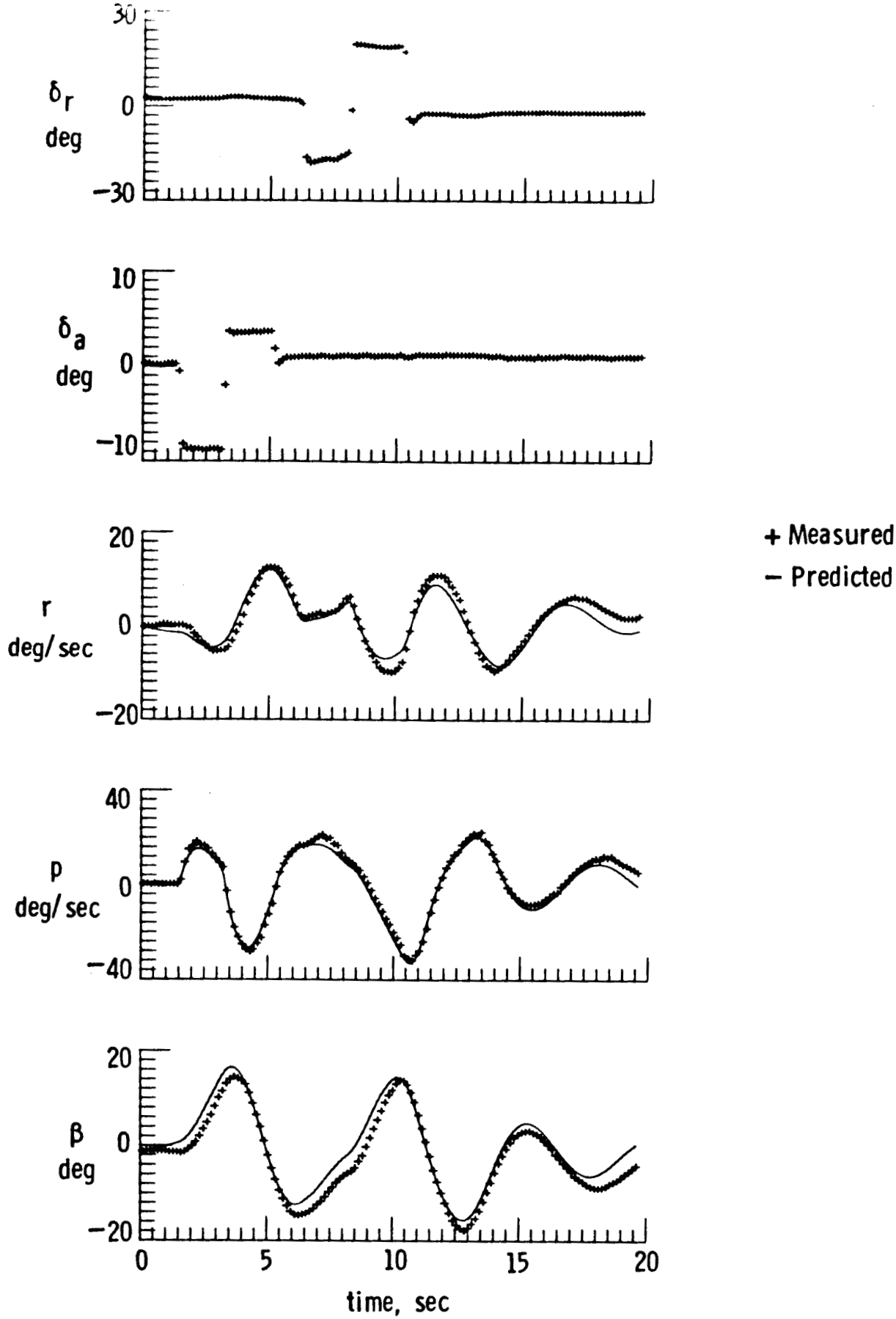

Figure 13b.- Comparison of Measured and Predicted Lateral Time Histories for SLE Modified Wing

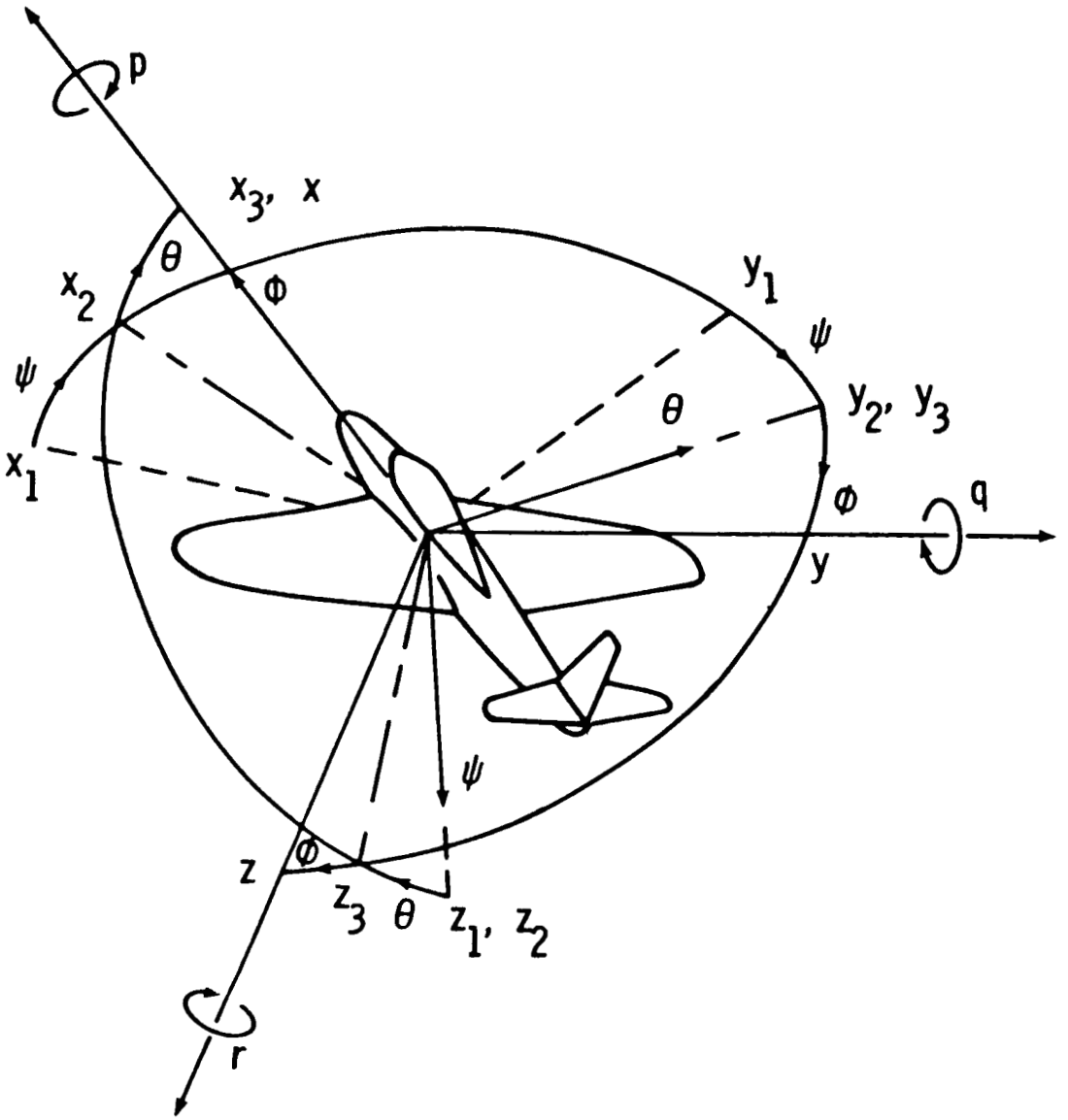

Figure 14.- Attitude Angle Reference System

1. Report No.	2. Government Accession No.	3. Recipient's Catalog No.
NASA TM-87591		

4. Title and Subtitle	5. Report Date
EFFECTS OF WING MODIFICATION ON AN AIRCRAFT'S AERODYNAMIC PARAMETERS AS DETERMINED FROM FLIGHT DATA	January 1986
	6. Performing Organization Code 505-34-03-06
7. Author(s) Robert Alan Hess	8. Performing Organization Report No.
	10. Work Unit No.
9. Performing Organization Name and Address NASA Langley Research Center Hampton, VA 23665-5225	11. Contract or Grant No.
	13. Type of Report and Period Covered Technical Memorandum
12. Sponsoring Agency Name and Address National Aeronautics and Space Administration Washington, DC 20546	14. Sponsoring Agency Code

15. Supplementary Notes

16. Abstract

A study of the effects of four wing-leading-edge modifications on a general aviation aircraft's stability and control parameters is presented. Flight data from the basic aircraft configuration and configurations with wing modifications are analyzed to determine each wing geometry's stability and control parameters. The parameter estimates and aerodynamic model forms are obtained using the stepwise regression and maximum likelihood techniques. The resulting parameter estimates and aerodynamic models are verified using vortex-lattice theory and by analysis of each model's ability to predict aircraft behavior. Comparisons of the stability and control derivative estimates from the basic wing and the four leading-edge modifications are accomplished so that the effects of each modification on aircraft stability and control derivatives can be determined.

17. Key Words (Suggested by Author(s))	18. Distribution Statement
general aviation stall/spin parameter identification parameter estimation system identification	UNCLASSIFIED - UNLIMITED SUBJECT CATEGORY 08

19. Security Classif. (of this report)	20. Security Classif. (of this page)	21. No. of Pages	22. Price
UNCLASSIFIED	UNCLASSIFIED	72	A04

For sale by the National Technical Information Service, Springfield, Virginia 22161